

Multiple superbubbles in the starburst nucleus of NGC 5253? – Implications for mass loss from dwarf galaxies

David K. Strickland[★] and Ian R. Stevens[†]

School of Physics and Astronomy, The University of Birmingham, Edgbaston, Birmingham, B15 2TT, U.K.

Accepted; Received; in original form

ABSTRACT

We obtained a long *ROSAT* HRI observation of the nearby dwarf starburst and Wolf-Rayet galaxy NGC 5253. Our aim was to resolve the source of the soft thermal X-ray emission seen by the *ROSAT* PSPC, proposed to be a luminous superbubble by Martin & Kennicutt (1995). Instead of a single superbubble, we find a complex of at least five sources of X-ray emission, associated with the massive clusters of young stars at the centre of NGC 5253. The individual 0.1 – 2.4 keV X-ray luminosities of the components lie in the range $2 - 7 \times 10^{37}$ erg s⁻¹. Three of the components are statistically extended beyond the HRI PSF, the largest having a FWHM of 8_{-4}^{+10} arcsec, equivalent to 160_{-80}^{+200} pc. We consider the origin of the observed X-ray emission, concentrating on the sources expected to be associated with the starburst region: superbubbles, supernovae, supernova remnants and massive X-ray binaries. To assess the X-ray luminosity of a young superbubble blown by a single massive cluster of stars we perform hydrodynamical simulations with realistic time-varying mass and energy injection rates. The predicted soft X-ray luminosity for a superbubble blown by a $M_{\star} = 10^5 M_{\odot}$ cluster during its Wolf-Rayet period agrees very well with the luminosities inferred for the extended components seen by the HRI. We conclude that the extended X-ray components are most likely young superbubbles blown by individual young clusters in the starburst region. Although we do not rule out a contribution to the observed soft X-ray emission by SNRs and massive X-ray binaries, we argue that the majority of the emission comes from a few young superbubbles blown by the young stellar clusters in the starburst region. We discuss in detail the implications of multiple superbubbles on the efficiency of mass and metal ejection from dwarf galaxies by starburst driven galactic winds. We suggest the presence of multiple stellar clusters in starbursting dwarf galaxies and the resulting multiple superbubbles will reduce the total ISM mass ejected from dwarf galaxies compared to the current models which only consider the blowout of a single superbubble.

Key words: ISM: bubbles – ISM: jets and outflows – Galaxies: individual: NGC 5253 – Galaxies: starburst – Galaxies: star clusters – X-rays: galaxies.

1 INTRODUCTION

Starbursts are periods of enhanced star formation, generally in the central several hundred parsecs of a galaxy, that will exhaust the available gas supply in significantly less than a Hubble time. Starburst events in dwarf galaxies are particularly interesting as there is the potential for major mass loss from the galaxy and the ejection of a significant fraction

of the interstellar medium (ISM) due to superbubbles and galactic winds driven by the pressure of thermalised supernova and stellar wind ejecta from the massive stars created in the starburst.

The basic model for a starburst driven wind (*c.f.* Suchkov et al. 1994) is conceptually simple: The thermalised kinetic energy from massive stellar winds and SN ejecta in the starburst region create a hot, X-ray emitting bubble in the ISM of host galaxy. This expands, sweeping up and shock heating the ambient medium to form a superbubble. In a disk-like ISM this superbubble will break out of the disk after a few million years to form a bipolar galactic wind, as seen around M82 (Watson, Stanger & Griffiths 1984; Strick-

[★] Present address: The Department of Physics & Astronomy, Johns Hopkins University, 3400 North Charles Street, Baltimore, MD 21218, USA. E-mail: dks@eta.pha.jhu.edu

[†] E-mail: irs@star.sr.bham.ac.uk

land, Ponman & Stevens 1997). In dwarf galaxies with less disk-like ISMs, the superbubble may sweep up and accelerate a significant fraction of the ISM to escape velocity (De Young & Heckman 1994) before blowing out into the intergalactic medium (IGM).

The loss of gas, and in particular material enriched with heavy elements due to nucleosynthesis in massive stars, has a range of cosmological implications: for the chemical evolution of dwarf galaxies (Bradamante, Matteucci & D'Ercole 1998 and references therein); their structure and evolution, possibly turning dI galaxies into dE galaxies (see Marlowe et al. 1997 for a detailed discussion) or disrupting them totally if they don't have massive dark haloes (Vader 1986; Dekel & Silk 1986); and for the chemical enrichment and heating of the Intra-Galactic medium (Spaans & Norman 1997).

The study of local starbursting dwarf galaxies has been invigorated by the discovery of low mass star forming galaxies at intermediate redshifts. Local starburst galaxies are readily accessible analogues of the star forming galaxies at higher redshifts, allowing the processes of galaxy evolution and formation to be investigated at a level of detail otherwise unobtainable.

Understanding the effect of starbursts on low mass galaxies requires quantitative measurements of the total energy and mass of gas (and newly synthesised heavy elements) incorporated into starburst-driven superbubbles and galactic winds, and how much of this escapes the galaxy, as a function of the properties of the host galaxy and the star formation rate.

X-ray observations provide the only direct probe of the hot, metal enriched, gas that fills most of the volume of superbubbles and contains most of the energy. Most of the mechanical energy injected by the stellar winds and supernovae into a superbubble is stored as thermal energy in the hot bubble interior. This hot phase also contains the newly synthesised heavy elements. Dense gas swept up and shock-heated by superbubbles and winds does emit optical emission lines, most notably $H\alpha$, but this is only an indirect probe of superbubbles and winds. The optical emission lines are predominantly excited by photoionisation from the massive stars (Martin 1997), making it much harder to study superbubbles with them. X-ray observations therefore provide the best single way to study starburst-driven superbubbles and galactic winds.

Characteristically, the X-ray emission from superbubbles and galactic winds is soft, $kT \sim 0.5$ keV. Although the specific energy of the supernova ejecta corresponds to a temperature $kT \sim 10$ keV if efficiently thermalised, hard X-ray emission from superbubbles and galactic winds will be much weaker than the soft X-ray emission from gas at several million degrees Kelvin. Thermal conduction and mass loading both introduce cooler and denser material into the interior of superbubbles, which dominate the X-ray emission as the luminosity is proportional to the square of the density (*c.f.* Weaver et al. 1977; Hartquist et al. 1986). In galactic winds much of the soft X-ray emission is believed to come from shock-heated clouds caught up in a faster moving, hotter but more tenuous wind (Suchkov et al. 1994).

Soft X-ray emission associated with the central regions and haloes of starburst galaxies is therefore taken as evidence of starburst-driven bubbles or winds. Diffuse X-ray emission is seen extending beyond the optical disks of some

of the nearest starburst galaxies such as M82 (Strickland et al. 1997), NGC 1569 (Heckman et al. 1995) and NGC 4449 (Della Ceca, Griffiths & Heckman 1997), with properties consistent with those expected of mature galactic winds.

The observational status of X-ray emission from younger starbursts, where the superbubbles are still confined within the disk of the galaxy, is more uncertain. *ROSAT* Position Sensitive Proportional Counter (PSPC) observations of dwarf star forming galaxies such as NGC 5253 (Martin & Kennicutt 1995), I Zw 18 (Martin 1996) and NGC 4861 (Motch, Pakull & Pietsch 1994) show unresolved soft X-ray sources coincident with their starburst regions. These are believed to be superbubbles on the basis of their soft thermal spectra and association with the starburst. Unfortunately, current X-ray instruments with the spectral-imaging capabilities necessary to identify superbubbles have, at best, only moderate spatial resolution. For example, the *ROSAT* PSPC's (the highest spatial resolution spectral-imager to have been flown at the time of writing)[†] spatial resolution of $\sim 30''$ corresponds to a physical size of ~ 600 pc at a distance of 4 Mpc, typical of a *nearby* starburst galaxy such as NGC 5253 or M82. This resolution is too low to resolve any young superbubbles, and hence higher resolution X-ray observations are required to establish the exact origin of the emission. Without high resolution X-ray observations, the exact source of the soft X-ray emission is unknown, and point source contamination of spectra also becomes a potential problem.

This ambiguous observational status is unfortunate, as the superbubble phase is important to study for several reasons:

(i) The dynamics of superbubbles are less complicated than those of mature galactic winds (*e.g.* Suchkov et al. 1994), which are not as well understood as those of superbubbles. As a result a quantitative understanding of superbubbles should be easier to achieve.

(ii) The superbubble phase is the best time to study the coupling between the massive stars formed in the starburst and the ISM they affect through superbubbles. Once the superbubble has blown out of the ISM into the IGM the interaction between the hot gas from the starburst and the remaining ISM is reduced, and as the wind expands into the halo the X-ray emission gets fainter as the density drops. The parent stellar population of a young superbubble will also be easier to identify and study.

(iii) Studies of the superbubble phase are important for calibrating and constraining the theoretical models necessary to understand the later, more complex, galactic wind phase and for obtaining quantitative estimates of the total mass and energy ejected from starburst galaxies. X-ray observations cannot be used on their own, as they provide ambiguous results. Standard single or two temperature spectral model fits to X-ray data do not accurately represent the complex multi-temperature gas distribution in superbubbles, as hence can not be used to accurately infer the

[†] The soon to be launched Advanced X-ray Astrophysics Facility (*AXAF*) will revolutionise this field, with a collecting area and spectral resolution far superior to *ROSAT*, and a spatial resolution of $\sim 0''.5$ (equivalent to ~ 10 pc at the distance of M82 or NGC 5253)!

true gas properties (see Strickland & Stevens 1998) on their own.

We decided to observe the nearby dwarf starburst galaxy NGC 5253 with the High Resolution Imager (HRI) on board *ROSAT*, with the aim of resolving and determining the origin of the soft X-ray emission seen by the *ROSAT* PSPC, believed to be a luminous superbubble (Martin & Kennicutt 1995).

NGC 5253 is an ideal target for several reasons:

- (i) It is widely acknowledged to be a very young starburst. Rieke, Lebofsky & Walker (1988) place it as the youngest starburst in their chronological sequence of starbursts based upon its high Br γ equivalent width. Its radio spectrum is almost entirely thermal, unlike many starburst galaxies, indicating very few classical supernova remnants (Beck et al. 1996). Spectral features due to Wolf-Rayet (WR) stars have been identified in two of the massive star clusters, constraining them to be only 3–5 Myr old (Schaerer et al. 1997).
- (ii) Soft X-ray emission attributed to a luminous superbubble had already been discovered in the *ROSAT* PSPC observation of Martin & Kennicutt (1995).
- (iii) It is one of the nearest Wolf-Rayet galaxies (Conti 1991) at a distance of 4.1 Mpc[§] (Saha et al. 1995). Wolf-Rayet galaxies are a class of young starburst galaxies, and are significantly X-ray overluminous compared to a sample of “normal” galaxies and more mature starbursts (Stevens & Strickland 1998a, 1998b). Their *ROSAT* PSPC spectra are best characterised as emission from a soft thermal plasma. One explanation for their excess X-ray luminosity is that it is due to young superbubbles, which later blow out of the galaxy and fade.

NGC 5253 therefore represents a chance to study at high resolution (the $\sim 5''$ resolution of the HRI corresponds to a physical size of 100 pc at the distance of NGC 5253) the X-ray properties of a very young starbursting dwarf galaxy, with a wealth of supporting observations at other wavelengths reported in the literature.

We shall briefly review previous X-ray observations of NGC 5253 in § 2, before describing our *ROSAT* HRI analysis in § 3 and our results in § 4. We detect at least five sources in the starburst region of NGC 5253, instead of the single superbubble expected. The possible sources of the five X-ray components are discussed in § 5, concentrating on superbubbles, supernovae, supernova remnants and massive X-ray binaries, given the association between the X-ray emission and the young massive stars in the starburst region. We conclude that multiple superbubbles blown by the massive clusters of young, recently-formed stars probably dominate the X-ray emission from NGC 5253. The implications of multiple superbubbles for starburst-driven mass loss from NGC 5253 and other dwarf galaxies are discussed in § 6, before summarising our conclusions in § 7.

[§] The Wolf-Rayet galaxy NGC 1569 is nearer than NGC 5253 at distance of only 2.2 Mpc, but is clearly an older and more evolved starburst galaxy with a complex star formation history and a well developed galactic wind (Vallenari & Bomans 1996; González Delgado et al. 1997).

2 PREVIOUS X-RAY OBSERVATIONS

NGC 5253 has previously been detected at X-ray wavelengths by both the *Einstein* IPC and the *ROSAT* PSPC.

Using a 34 ksec observation with the *ROSAT* PSPC, Martin & Kennicutt (1995) found a single marginally extended ($\sim 10''$) source. At a distance of 4.1 Mpc the physical size of this possible extended source is ~ 200 pc. The X-ray spectrum was well fit with a soft, $kT \sim 0.4$ keV, absorbed thermal plasma model, with a total 0.1–2.4 keV X-ray luminosity of $L_X \sim 7 \times 10^{38}$ erg s $^{-1}$.

A re-analysis of this data as part of a *ROSAT* sample of WR galaxies by Stevens & Strickland (1998) finds a slightly lower luminosity of $L_X \sim 4 \times 10^{38}$ erg s $^{-1}$, due to using a lower value for the absorbing column density.

A previous 6 ksec observation with the lower resolution and sensitivity *Einstein* IPC detected a source coincident with NGC 5253’s position with a count rate that corresponds to a 0.1–2.4 keV X-ray luminosity of $L_X \sim 5 \times 10^{38}$ erg s $^{-1}$, consistent with *ROSAT* PSPC observations assuming the same spectral model. (Fabbiano, Kim & Trinchieri 1992).

Considering the various possible sources of the X-ray emission Martin & Kennicutt (1995) provisionally attributed it to hot gas in a superbubble, heated by supernovae and stellar winds from the young stars created in the starburst.

3 HRI DATA REDUCTION AND ANALYSIS

NGC 5253 was observed by the *ROSAT* HRI (David et al. 1996) for 71472 s between the 25th to 28th, July 1996. The data was reduced and analysed using the ASTERIX X-ray analysis package. For a detailed description of the *ROSAT* HRI see David et al. (1996) or Briel et al. (1994). After screening for periods of poor pointing accuracy (a negligible reduction) and dead-time time correction, the effective exposure time on axis is 71003 s.

The HRI has only a crude spectral sensitivity, although it is possible to generate hardness ratios (Wilson et al. 1992). The pulse height analyser (PHA) distribution of the HRI background, which is mainly particle events as opposed to the soft X-ray background, differs from the PHA distribution of X-ray sources. To reduce the background we used only data between PHA channels 3 and 8, inclusive. This maximises the sensitivity for point sources and low surface brightness diffuse features. Using only these channels reduces the background rate by $\sim 25\%$ to 8.2×10^{-7} counts s $^{-1}$ arcsec $^{-2}$ from the nominal rate of 1.1×10^{-6} counts s $^{-1}$ arcsec $^{-2}$.

3.1 Sources and positional accuracy

The absolute positions of *ROSAT* HRI sources are only accurate to $\sim 6''$ (c.f. Briel et al. 1994; David et al. 1996). This corresponds to an physical uncertainty of ~ 120 pc assuming the distance to NGC 5253 is 4.1 Mpc. This uncertainty can be reduced if X-ray sources within the field of view can be identified with objects at other wavelengths, where usually the positions are known with better accuracy (see, among many examples, Wang 1995).

We used the maximum likelihood point source searching

algorithm Pss to find sources more than 4σ above the background, over the entire HRI field of view. Several methods of estimating the background were used, but all gave essentially the same resulting source list, apart from the most marginal detections. Excluding NGC 5253 itself, 31 sources were found. We will discuss the sources within the optical confines of NGC 5253 below.

We cross-correlated our HRI source list (excluding NGC 5253 itself) with all sources within the same region of sky from SIMBAD, the Nasa Extragalactic Database (NED), the HST Guide Star Catalogue (GSC) and those X-ray sources detected in the PSPC observation. In addition we cross-correlated the HRI source list with the positions of any object seen, in a Digitised Sky Survey (DSS) image of the HRI field of view, that lay within $30''$ of a HRI source.

No correlation with any source in the SIMBAD and NED databases was found, including the two historical SN Ia in NGC 5253. Five of the sources were detected in the PSPC observation. The offsets and bearings of the nearest optical source from the DSS image for each X-ray source are random.

For a maximum correlation distance of $20''$, only one correlation between our HRI source list and the GSC was found. One of the brightest X-ray sources in the field of view, a 7σ detection (also seen in the PSPC observation) was offset from the position of the Guide Star 072660005 ($\alpha_{2000.0} = 13^{\text{h}}39^{\text{m}}50^{\text{s}}.69$, $\delta_{2000.0} = -31^{\circ}34'11''.6$) by $\Delta\alpha = +2''.7$, $\Delta\delta = +1''.8$.

We have corrected the nominal HRI pointing solution to align the X-ray source with the GSC star position. It is worth noting that with only one cross-correlation we cannot assess if the nominal HRI pointing solution is rotated with respect to the GSC. We regard the absolute X-ray positions quoted in this paper to be more accurate than the nominal HRI uncertainty of $\sim 6''$, although no more accurate than $\sim 3''$.

3.2 Image analysis

For the analysis of the soft X-ray emission from NGC 5253 itself data from the central $0''.03 \times 0''.03$ was binned into $1''$ square pixels, and corrected for vignetting, dead-time and exposure time.

Visual inspection of the lightly smoothed image (Fig. 1) reveals at least five, *apparently point-like* sources of emission, over a $25'' \times 30''$ (500 pc \times 600 pc) region.

To quantify the X-ray emission we used a maximum likelihood image fitting program to fit for the positions and intensities of five point sources (modeled using the functional form of the *ROSAT* HRI point spread function [PSF]) and the intensity of a flat background to the data. We used a maximum likelihood method, rather than a traditional χ^2 technique, given the low number of counts in each component.

To ease the fitting process, we supplied the fitting program a first guess at the positions and fluxes of the five components. The background count rate at the position of NGC 5253 was extrapolated from a polynomial fit to the radial profile of the source-subtracted image of the entire HRI field of view. The inner $0''.04$ was excluded to avoid biasing the polynomial fit by any kiloparsec-scale low surface brightness diffuse emission that may be present near NGC

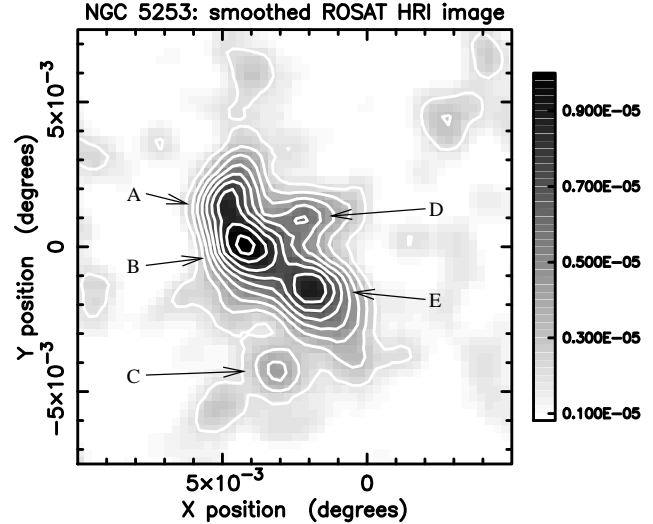


Figure 1. Smoothed exposure corrected HRI X-ray image of NGC 5253. The data was binned in $1''$ square pixels, and smoothed with a Gaussian mask of FWHM $4''.7$. Units are $\text{counts s}^{-1} \text{arcsec}^{-2}$. The letters refer to the X-ray components identified in the text and in Table 1. The contour levels begin at a surface brightness of $2 \times 10^{-6} \text{ counts s}^{-1} \text{arcsec}^{-2}$, and increase linearly in increments of $10^{-6} \text{ counts s}^{-1} \text{arcsec}^{-2}$.

5253. The estimated background level was $2.95 \pm 0.10 \times 10^{-3}$ $\text{counts s}^{-1} \text{arcmin}^{-2}$. We shall return to the question of any larger scale diffuse X-ray emission later, after first considering the five observed components in more detail.

To gain some insight into the origin of the X-ray emission, we have overlaid a contoured HRI image on a HST WFPC2 image (see Fig. 2a, courtesy of V. Gorjian, originally published in Gorjian 1996). This shows that the soft X-ray emission comes from the starburst region near the centre of NGC 5253, and the most intense emission is apparently associated with the massive young stellar clusters.

The brightest X-ray component B (identified in Fig. 1) is only slightly offset to the east from the brightest cluster seen in the optical. This cluster is bright enough to qualify as a “Super Star Cluster” (SSC, Meurer et al. 1995). SSCs are possibly the progenitors of globular clusters, and are found in many starburst galaxies. Another bright cluster of young stars is only $\sim 3''$ to the SW of the SSC.

The second brightest X-ray component E is also almost on top of two slightly less massive clusters. The properties of the optical clusters are discussed in greater depth in § 5.5.

The southern-most X-ray component C is also associated with a more diffuse association of massive stars or lower mass clusters. The brightness of the main clusters makes this difficult to show in Fig. 2a. This southern grouping of massive stars is more visible in the ground based optical images kindly supplied to us by C. Martin (Fig. 2c, first published in Martin & Kennicutt 1995), or as a local peak in the $\text{H}\alpha$ emission (Fig. 2d, Martin & Kennicutt 1995, or Fig. 1b of Calzetti et al. 1997).

The northern-most components A & D are not obviously associated with any bright clusters. Together with component B, components A & D appear to make a broken ring-shaped structure open to the north. We regard this

as spurious, and choose to consider them as three separate components.

On the larger scale, the soft X-ray emission is clearly confined well within the optical extent of the galaxy, and is less extended than the ~ 1 kpc scale H α filament complex (Fig. 2b – d).

A comparison between this WFPC2 image and other optical, UV and radio observations can be found in Gorjian (1996). Readers may also find it useful to compare Fig. 2 with the optical and H α images published in Calzetti et al. (1997).

The coordinate systems for the optical images in Fig. 2 have been adjusted so that the main starburst clusters have the positions quoted in Calzetti et al.'s (1997) study of all the HST observations of NGC 5253.

3.3 Source sizes

As can be seen in Figs. 1 & 2a, some of the components seem physically larger and more extended than others. In particular the peaks of components C, E & B appear much broader than those of components A & D. In order to quantify the level to which the HRI data constrain the sizes of the individual components, we replaced the point-source model for individual X-ray components with a model consisting of a Gaussian source blurred by the HRI PSF.

Can we realistically expect to constrain the size of the individual components, given we only have between ~ 20 and ~ 45 counts in each of the components, and any extension is similar to the size of the ROSAT HRI PSF (HWHM $\approx 2.8'$, David et al. 1996)?

We performed a set of simulations to assess whether it is possible to resolve marginally extended sources (*i.e.* HWHM = 1 – 5''), for source and background count rates appropriate to our NGC 5253 observation. The Gaussian model, convolved with the HRI PSF, was used to produce simulated sources, of chosen size (HWHM in the range 0.5' to 5.0') and count rate, on top of a flat background. Adding Poisson noise, and then exposure correcting, gave an artificial observation which was fitted with the original model of a flat background and Gaussian source blurred by the HRI PSF. Several different Poisson realisations were made for each size model.

For simulated sources having a similar total number of counts to the brighter X-ray components B & E, it is possible to distinguish weakly resolved (HWHM $\gtrsim 1''$) from unresolved sources with a typical uncertainty in HWHM of $\sim 1''$. For fainter sources, similar to components C & D, only larger sources (HWHM $\gtrsim 3''$) can be distinguished as being inconsistent with the HRI PSF.

On this basis, we expected components B, C & E to be the best candidates for showing any true source extension, given that components B & E are the brightest, and component C, although fainter, appears large and is not in the wings of the brighter components as components A & D are. From the simulations we felt confident that our HRI data could be used to distinguish between truly unresolved point-sources and weakly extended sources, for at least a few of the observed components, and place meaningful limits on their sizes.

Rather than attempt to directly fit five Gaussians and a background level to the data, we adopted the more ‘hands-

on’ method described below, given the low count rates, complexity of the large fit parameter space and potential for false minima.

We stepped individually through the components, replacing the point source model with a Gaussian model at the point-source best-fit position. The other four components were fixed at their best-fit point source positions and fluxes. We then investigated the variation in best-fit Cash C-statistic (Cash 1979) with Gaussian size (as parameterised by the HWHM, between 0.5' and 15''), fitting for position and both the Gaussian and the background-level normalisation.

Only components B, C & E showed any evidence for significant minima at non-zero extension, with best-fit Cash statistic values that improved on the best-fit five point source model. The best-fit total flux for these components also increased, indicating that the point source model was missing flux. However, replacing only one component at a time with the Gaussian model, and leaving the remaining components as point-sources is less than ideal, given that three components showed signs of being extended. Some, although not all, of the apparent extension could be due to the Gaussian model picking up flux from the other extended sources that the point source model missed.

We then replaced the best-fit point source models for components B, C & E with the best-fit Gaussian models, and then re-ran the procedure detailed above of stepping through all the components, replacing each in turn with a Gaussian model and investigating how the Cash statistic varies with Gaussian HWHM. As experiment showed that the best-fit positions were not altering, they were fixed at this point, and not fitted for again. Components A & D remained statistically unresolved, while components B & C were reduced in size. Component E remained almost the same size. The change in Cash statistic ΔC (equivalent to $\Delta\chi^2$) from the minimum value found as a function Gaussian HWHM for each component is shown in Fig. 3.

After updating the current best-fit model (two point sources, three Gaussians and the background normalisation), we finally fitted for the normalisation of all the components, and the size of the three Gaussian models, as we were confident that we had stepped as close to the true fit minimum as possible. The final best-fit parameters and 90% confidence regions for the five components are given in Table 1. For components A & D, we place upper limits on their size (shown in Table 1) by estimating the Gaussian HWHM for a $\Delta C = 2.71$.

It is unlikely that the apparent extension of the X-ray components is due to any systematic error in either our fitting process, or a systematic blurring of the HRI PSF in the data (*e.g.* the spatial smearing discussed by Harris et al. 1998). If this were the case, we would expect to see all five components to show approximately the same extension, which is clearly not the case.

4 RESULTS

4.1 X-ray emission from within NGC 5253

Assuming all the sources are spectrally similar, the best-fit spectral model from the *ROSAT* PSPC observation can be used to convert HRI count rates to X-ray luminosities.

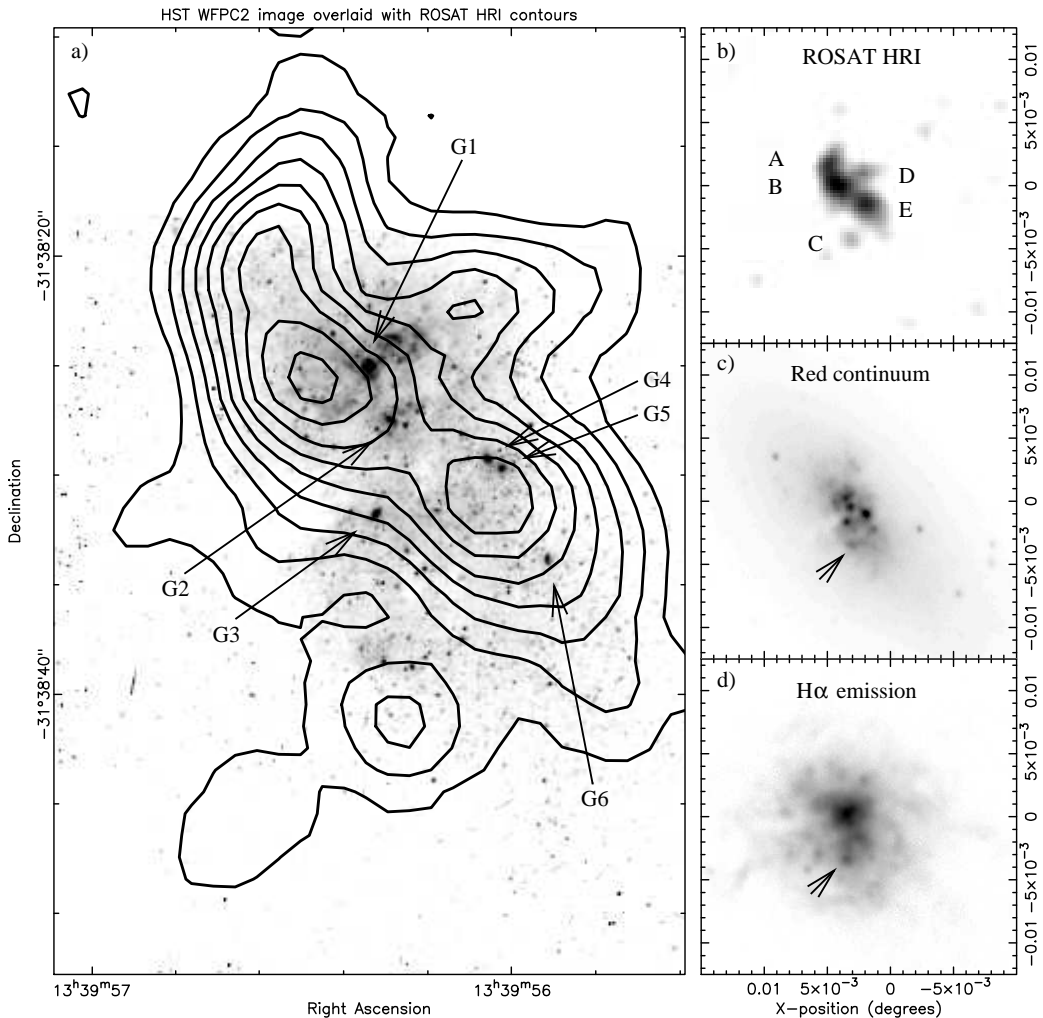


Figure 2. (a) A HST WFPC2 image of the centre of NGC 5253 (courtesy of V. Gorjian, 1996) overlaid with a lightly smoothed contour map of the soft X-ray emission seen by the *ROSAT* HRI (with the same contour levels as in Fig. 1). The bright star clusters from Table 2 have been marked on the image. The intensity scale of the optical image has been adjusted to show only the young massive stars and clusters of the starburst region. The distribution of the X-ray emission with respect to the stars and ionised gas on a larger scale can be seen in (b) – (d). These show on the same scale the X-ray emission (b), ground-based red continuum (c) and (d) H α images (courtesy of C. Martin, see Martin & Kennicutt 1995). The arrow in (c) & (d) highlights the diffuse southern group of massive stars possibly associated with X-ray component C, discussed in § 3.2. The absolute registration of the X-ray image with respect to the optical images is uncertain to $\sim 3''$, as discussed in § 3.

As described in § 2, Martin & Kennicutt (1995) found that the *ROSAT* PSPC spectrum was well described by a soft Raymond-Smith hot plasma model (Raymond & Smith 1977) of temperature $kT \approx 0.34 \pm 0.10$ keV, assuming a total absorbing column of $N_{\text{H}} = 2.5 \times 10^{21} \text{ cm}^{-2}$ (based on examination of HI maps and the visual extinction towards to core on NGC 5253). Stevens & Strickland (1998a) got very similar results, $kT \approx 0.43$ keV and $N_{\text{H}} = 8_{-4}^{+10} \times 10^{20} \text{ cm}^{-2}$ (fitting for the hydrogen column).

Assuming a Raymond-Smith hot plasma model for the X-ray emission, based on the results quoted above, of temperature $T = 0.4$ keV and metallicity $Z = 0.25Z_{\odot}$, and correcting for a total absorbing column (*i.e.* Galactic and that intrinsic to NGC 5253) of $N_{\text{H}} = 10^{21} \text{ cm}^{-2}$, a 0.1–2.4 luminosity of $L_{\text{X}} = 1.15 \times 10^{41} \text{ erg s}^{-1}$ corresponds to one count per second in the *ROSAT* HRI. For the Galactic

column of $N_{\text{H}} = 4.0 \times 10^{20} \text{ cm}^{-2}$ (Dickey & Lockman 1990), one HRI count per second corresponds to a luminosity of $L_{\text{X}} = 8.73 \times 10^{40} \text{ erg s}^{-1}$. The inferred intrinsic X-ray luminosities are given in Table 1, and range between $2 - 7 \times 10^{37} \text{ erg s}^{-1}$ for the different components. Note that the errors in L_{X} reflect only the uncertainties in the count rates, and not those in the spectral model itself. The count rate to luminosity conversions quoted above, and hence the inferred X-ray luminosities of the five X-ray components, are sensitive to the assumed spectrum and the assumed column density.

We have assumed a typical absorption column of $N_{\text{H}} = 10^{21} \text{ cm}^{-2}$ based on the fitted column of Stevens & Strickland (1998a), although the absorption may be a few times higher than that, as assumed by Martin & Kennicutt (1995). The peak hydrogen column density in centre of NGC 5253,

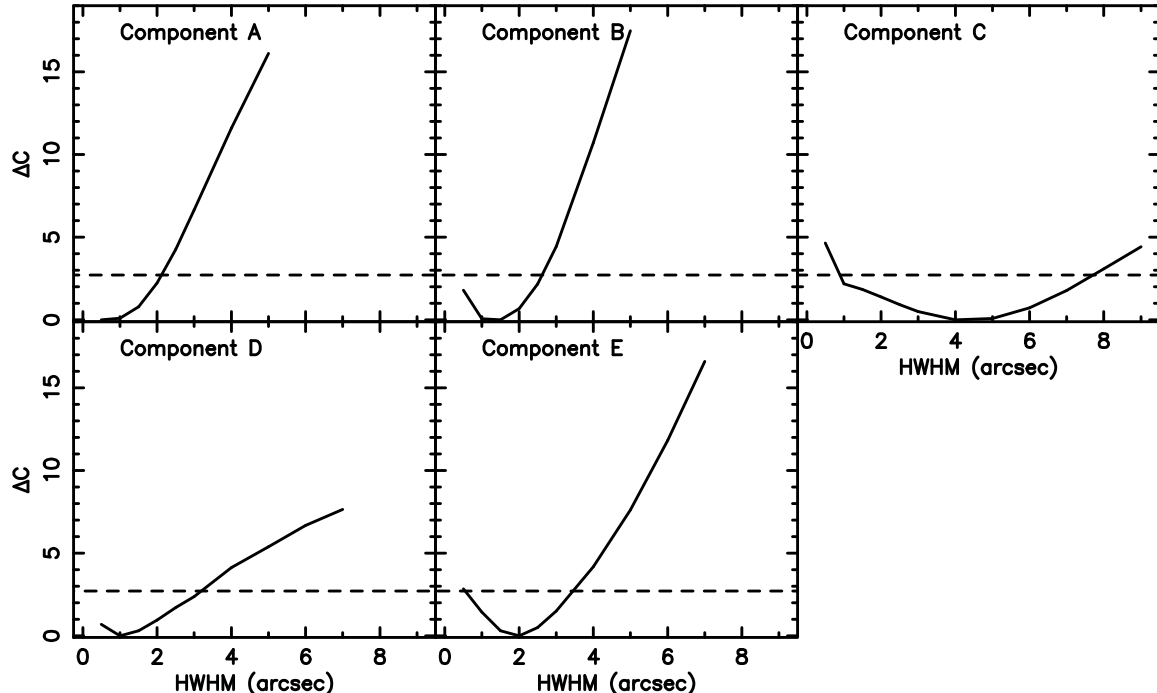


Figure 3. The shape of the fit surface near the fit minimum for a Gaussian model (convolved with the HRI PSF) fit to each X-ray component. The plots show the change in Cash C-statistic from the best-fit value, ΔC (equivalent to $\Delta\chi^2$), as a function of the Gaussian HWHM. For each component, the models for the other four components are fixed at their best-fit values (see the text for details). Components A & D are consistent with being unresolved, *i.e.* point sources, while components B, C & E are consistent with being marginally extended (HWHM in the range 1.5 to 4 arcsec) with respect to the HRI PSF (which has a HWHM ≈ 2.8 , David et al. 1996). The intersection of the dashed line shown at $\Delta C = 2.706$ with the fit surface represents the 90% confidence interval in HWHM.

beam-averaged over a region ~ 1 kpc in size, from the HI measurements of Kobulnicky & Skillman (1995) is $N_{\text{H}} = 2.6 \times 10^{21} \text{ cm}^{-2}$. If we assume the neutral hydrogen is uniformly distributed in front of and behind the central starburst region, the net absorbing column experienced by X-ray photons from the core of NGC 5253 is $N_{\text{H}} \sim 1.7 \times 10^{21} \text{ cm}^{-2}$. Note that the HST-based study conducted by Calzetti et al. (1997) has shown that the optical extinction in the starburst region is very patchy, from regions with almost no absorption to regions hidden behind 10 – 30 magnitudes of optical extinction (equivalent to hydrogen columns of $N_{\text{H}} \sim 2 \times 10^{22} – 6 \times 10^{22} \text{ cm}^{-2}$ based on the conversion between hydrogen column and visual extinction published in Gorenstein 1975). However emission from extended sources of size a few arcseconds ($\gtrsim 100$ pc), such as components B, C & E, is less affected by localised patches of dust and high extinction. In the absence of more information regarding the origin and distribution of the X-ray emission from NGC 5253 our assumed hydrogen column of $N_{\text{H}} = 10^{21} \text{ cm}^{-2}$ is by no means unreasonable.

What limits can be placed on the X-ray luminosities of the individual X-ray components seen in the HRI observation? Assuming only the galactic hydrogen column, *i.e.* no absorption intrinsic to NGC 5253, gives a rough lower limit on the 0.1 – 2.4 keV X-ray luminosity (as given in Table 1). This lower limit is only approximate, as it does not account for the uncertainty in the true source spectrum for each source.

If $N_{\text{H}} \sim 2 \times 10^{21} \text{ cm}^{-2}$ then the 0.1 – 2.4 keV X-ray luminosities of the individual X-ray components seen by the HRI are a factor 1.44 times those given in Table 1. For a

column of $N_{\text{H}} = 2 \times 10^{22} \text{ cm}^{-2}$ the intrinsic X-ray luminosities are nearly two orders of magnitude higher than those given in Table 1, but note that such high columns are inconsistent with the results of the spectral fits to the *ROSAT* PSPC spectrum, and the assumed soft thermal model overestimates the intrinsic X-ray luminosity if the true hydrogen column was as high as high or higher than $2 \times 10^{22} \text{ cm}^{-2}$.

Is it safe to assume that all the sources have similar X-ray spectra? The *ROSAT* HRI has a limited spectral capability (Wilson et al. 1992; David et al. 1996). Wilson et al. used the ratio of PHA channels 1–5 over 6–11 to define a softness ratio. We created smoothed maps in channels 3–5 (soft) and 6–8 (hard), and created a hardness map, (soft-hard)/(soft+hard). With the low number of counts no evidence for significant hardness variations between the X-ray emitting components could be found.

4.2 Extended diffuse emission

Is there any evidence for diffuse X-ray emission on larger scales, as might be expected given the kiloparsec-scale H α filament complex (Marlowe et al. 1995, Martin & Kennicutt 1995)? Smoothed X-ray images show no obvious diffuse emission above the noise (Fig. 1), but the best-fit background level in the central 0.03×0.03 is significantly higher than that estimated using an source free annulus and correcting for the HRI vignetting function.

Using this background region, the estimated background level at the centre of the field is $2.95 \pm 0.10 \times 10^{-3}$ counts $\text{s}^{-1} \text{ arcmin}^{-2}$.

From the image fitting, there is a statistically significant

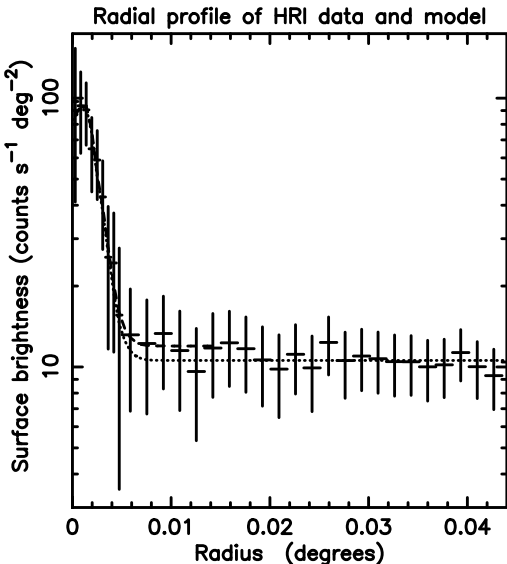


Figure 4. A radial profile of the *ROSAT* HRI data, overlaid with the radial profile predicted by the best-fit model to the data (dashed) shown to a radius of $0^{\circ}015$, within which the model was fitted. The dotted line shows the five component model with the expected background level, which clearly fits the data for $R \gtrsim 0^{\circ}02$. There is some evidence for excess flux above the expected background level for $R \lesssim 0^{\circ}02$ (~ 1 kpc), similar to the maximum extent of the $\text{H}\alpha$ emission.

excess (at the 3σ level) of $12.3 \pm 0.9 \times 10^{-4}$ counts s^{-1} (87 ± 6 counts) not accounted for by expected background and the five point sources themselves. This corresponds to an intrinsic X-ray luminosity of $1.1 \pm 0.1 \times 10^{38}$ erg s^{-1} , assuming $kT = 0.4$ keV, $Z = 0.25 Z_{\odot}$ and $N_{\text{H}} = 4 \times 10^{20}$ cm $^{-2}$.

This is too large an excess to be explained by any inadequacies of our PSF model for the HRI. It is difficult to assess whether the excess flux is associated with a genuine low surface brightness diffuse component, or is flux missed from the central point-like components by using only a five component fit to the data. A radial profile centred on the saddle point between components B & E does seem to suggest excess diffuse emission extending out to a radius of $\sim 0^{\circ}015$ (~ 1 kpc). A combination of future *AXAF* and *XMM* observations will tell us more.

4.3 Summary of observational results

In summary the HRI observations show several, at least five, separate sources of soft, 0.1–2.4 keV, X-ray emission, associated with the recent star formation at the centre of NGC 5253. The integrated X-ray spectrum observed by the *ROSAT* PSPC is best characterised as a soft thermal plasma, absorbed by a total column in excess of the galactic hydrogen column, and with possible sub-solar metal abundance. Within *ROSAT*'s pointing accuracy the brightest X-ray components are associated with the four brightest young clusters of massive stars, and the southern-most X-ray component is close to a more diffuse association of massive stars. Based on the PSPC spectrum the luminosities of the five components range between $L_{\text{X}} \approx 2 - 7 \times 10^{37}$ erg s^{-1} . Three of the components are statistically extended beyond the HRI PSF at 90% confidence, the largest having a FWHM of 8_{-4}^{+10}

arcsec, equivalent to 160_{-80}^{+200} pc. The upper limits on the sizes of the other two X-ray components are consistent with the sizes observed for the two brightest components that are extended, so we cannot rule out the possibility that they are marginally extended as well.

5 DISCUSSION

Martin & Kennicutt (1995), in their study of NGC 5253 using the *ROSAT* PSPC, argued that the most likely source of the X-ray emission was from a luminous superbubble evolving in a cloudy medium. A *ROSAT* PSPC survey of 14 Wolf-Rayet galaxies (including NGC 5253) by Stevens & Strickland (1998a; 1998b), also concluded that the source of the X-ray emission in these objects was most probably young superbubbles.

Given that with higher resolution the X-ray emission comes from several components it is worth re-assessing the possible sources of the observed emission.

5.1 X-ray emission from the massive stars

Individual O stars typically emit a fraction $L_{\text{X}}/L_{\text{Bol}} \sim 3 \times 10^{-7}$ of their total bolometric luminosity in soft X-rays, although with a scatter of about an order of magnitude around this mean value (Sciortino et al. 1990).

Using published data from the literature we can estimate the X-ray luminosities of the massive clusters of young stars in NGC 5253 due to soft X-ray emission from the massive stars alone. Table 2 collates the observed properties of the six brightest clusters in NGC 5253 (the brightest an example of a Super Star Cluster) from the work of Meurer et al. (1995), Gorjian (1996), Calzetti et al. (1997) and Schaerer et al. (1997).

From the estimated bolometric luminosities $L_{\text{bol}} \sim 10^{40} - 3 \times 10^{42}$ erg s^{-1} it is clear that individual massive stars cannot be the source of the soft X-ray emission seen in NGC 5253.

5.2 Massive X-ray binaries

Massive X-ray binaries (MXRBs) generally have hard X-ray spectra. That NGC 5253's X-ray spectrum is well fit by a soft thermal plasma model indicates that the majority of the X-ray emission is not produced by MXRBs.

MXRBs with a black hole (BH) rather than a neutron star are a possible source of the X-ray emission from the non-extended components, as they have a soft spectral component in addition to a hard power law tail, and can have luminosities up to $L_{\text{X}} \sim 10^{38}$ erg s^{-1} . The two strongest X-ray point sources within 30 Doradus may be Wolf-Rayet + BH binaries (Wang 1995).

The extension of X-ray components B, C & E and their dominance of the total count rate argue against all their emission being due to MXRBs and/or BH-binaries. MXRBs and BH-binaries could well provide some fraction of the total X-ray emission from NGC 5253. Higher resolution observations with the $0''.5$ resolution of *AXAF* will be necessary to identify what fraction of the soft X-ray emission comes from point sources.

Table 1. Best-fit parameters for the NGC 5253 HRI data. Errors quoted are 90% confidence in one parameter of interest for count rates and size.

Comp.	α (2000.0)	δ (2000.0)	Count rate (10^{-4} counts s $^{-1}$)	L_X^a (10^{37} erg s $^{-1}$)	L_X^b (10^{37} erg s $^{-1}$)	size (HWHM) (arcsec) c,d
A	13 ^h 39 ^m 56 ^s .52	-31 ^o 38'17"5	4.1 $^{+1.5}_{-1.5}$	3.6 $^{+1.3}_{-1.3}$	4.7 $^{+1.7}_{-1.7}$	< 2.0
B	13 ^h 39 ^m 56 ^s .35	-31 ^o 38'24"7	6.3 $^{+2.1}_{-1.9}$	5.5 $^{+1.8}_{-1.7}$	7.3 $^{+2.4}_{-2.2}$	1.4 $^{+1.3}_{-1.4}$
C	13 ^h 39 ^m 56 ^s .14	-31 ^o 38'40"2	3.4 $^{+2.6}_{-1.8}$	2.9 $^{+2.3}_{-1.6}$	3.9 $^{+3.0}_{-2.1}$	4.2 $^{+4.9}_{-2.3}$
D	13 ^h 39 ^m 55 ^s .75	-31 ^o 38'20"8	2.4 $^{+1.3}_{-1.2}$	2.1 $^{+1.1}_{-1.1}$	2.7 $^{+1.5}_{-1.4}$	< 3.0
E	13 ^h 39 ^m 55 ^s .68	-31 ^o 38'29"8	6.3 $^{+2.0}_{-2.0}$	5.5 $^{+1.8}_{-1.7}$	7.3 $^{+2.3}_{-2.2}$	1.9 $^{+1.1}_{-1.3}$

(a) Intrinsic 0.1–2.4 keV luminosity assuming a Raymond-Smith hot plasma model with $kT = 0.4$ keV, metallicity $Z = 0.25Z_\odot$, corrected for a Galactic absorbing column of $N_{\text{H}} = 4 \times 10^{20}$ cm $^{-2}$.

(b) As (a) except for a total $N_{\text{H}} = 10^{21}$ cm $^{-2}$.

(c) At a distance of 4.1 Mpc, 1 arcsecond corresponds to 20 pc.

(d) Positions and fluxes for components A & D are from a point source fit, with upper limits on size based on a Gaussian model fit. Otherwise best fit parameters are from fits to the data of a Gaussian source blurred by the HRI point spread function.

Table 2. Properties of the six brightest SSCs in NGC 5253, taken from Meurer et al. (1995, M95), Gorjian (1996, G96), Calzetti et al. (1997, C97) and Schaefer et al. (1997, S97). Masses quoted are the total initial mass between the two mass limits assuming a Salpeter IMF. The names and numbers used here and in Fig. 2 have been prefixed by the first letter of the first author's name to reduce confusion between their different naming conventions. We have used the Leitherer & Heckman (1995, LH95) instantaneous starburst models (for a Salpeter IMF and a metal abundance of 0.25 Solar) to estimate the bolometric luminosities and some of the masses.

Parameter	Cluster name						Ref. G96	Notes
	G1	G2	G3	G4	G5	G6		
	SA	SB						
	C5	C4	C1	C2	C3	C6	C97	
Age (Myr)	2.8	4.4					S97	
$\log N_{\text{LyC}}(\text{s}^{-1})$	52.0	51.4					S97	a
N_{O}	~ 1700	~ 840					S97	b
N_{WR}	~ 35	~ 52					S97	c
$\log M_\star$ (0.1–100 M_\odot)	6.0	5.7						d,e
R (pc)	3.3	3.0	3.1	2.2	1.5	1.7	G96	
Age (Myr)	2.2–2.8	4.0–4.4	8–12	50–60	30–50	10–17	C97	f,h
$\log M_\star$ (0.1–100 M_\odot)	5.5–6.0	4.0–4.6	4.8–5.6	4.8–5.6	4.8–5.6	4.8–5.6	C97	d,i
$\log L_{\text{bol}}$ (erg s $^{-1}$)	42.5	41.5	41.0	40.0	40.2	40.8		j
$\log M_\star$ (0.1–100 M_\odot)	≥ 3.8	≥ 4.4	≥ 4.3	≥ 3.8	≥ 3.9	≥ 4.0	M95	d,k

(a) Ionising Lyman continuum flux estimated from $H\beta$. Extinction dependent.

(b) Total number of O stars.

(c) Total number of Wolf-Rayet (WR) stars.

(d) Total mass in stars with masses between 0.1 and 100 M_\odot assuming a Salpeter IMF.

(e) Estimated here using inferred ages and number of O stars with the LH95 models.

(f) For clusters G1 & G2 the estimated age is based on $H\alpha$ & $H\beta$ equivalent widths.

(h) Age estimates based on cluster colours.

(i) Based on de-reddened absolute magnitude.

(j) Calculated from the LH95 models, assuming an initial mass of $10^6 M_\odot$ for G1 and $10^5 M_\odot$ for G2 – G6, and the youngest age estimate for each cluster.

(k) Assuming clusters are at peak UV brightness, and uniform reddening

5.3 Low-mass X-ray binaries

Low mass X-ray binaries (LMXBs), although having softer X-ray spectra than MXRBs, are still generally harder than the $kT \sim 0.4$ keV emission seen by the *ROSAT* PSPC. In addition, the association between the HRI X-ray sources and

the clusters of young massive stars argues against LMXBs being the sources of the observed emission.

5.4 Supernovae and Supernova Remnants

A natural consequence of the starburst phenomenon is a high supernova (SN) rate for tens of millions of years within a relatively small volume of the host galaxy.

SN occurring within cavities or bubbles blown by preceding SN or stellar winds are best considered within the framework of the superbubble model, discussed at length in § 5.5. Individual SN and SN remnants (SNR) can be luminous X-ray sources in their own right, which we shall consider here.

We can estimate the SN rate in NGC 5253 from an assumed star formation history. Meurer et al. (1995) estimate a total initial mass of $4.4 \times 10^6 M_\odot$ (for a Salpeter IMF extending between $0.1 - 100 M_\odot$) based on the average mass-to-light ratio for a constant star formation rate with an age between $1 - 100$ Myr. For ages between $10 - 50$ Myr the resulting SN rate is $\sim 10^{-3} \text{ yr}^{-1}$ and is not very sensitive to the star formation history.

No type II SN have been observed in NGC 5253, although two SN Ia have occurred in the outer parts of the galaxy (Saha et al. 1995). The radio spectrum of NGC 5253 places upper limits on the total number of classical SN or SNR, as it is unusual for a starburst galaxy in being almost entirely thermal (90% – 95%) in origin, suggesting very few if any isolated SN & SNRs (Beck et al. 1996). These measurements would have detected the presence of 10 or more SNRs, or a single radio SN. The arcsecond resolution radio observations show only one compact (but not point-like) radio source, associated with the very young and bright cluster G1 (adopting the naming convention from Table 2).

Young (ages measured in decades) type II SN have a wide range of X-ray luminosities, from $L_X \sim 2 \times 10^{35} \text{ erg s}^{-1}$ for SN1987A in the *ROSAT* band, to several $\times 10^{40} \text{ erg s}^{-1}$ for SN1986J and SN1993J (Schlegel 1995 and references therein). With no SN IIs observed within the last century it seems unlikely that any of the observed X-ray emission is due to recent SN.

In general SNRs are faint X-ray sources, with $0.1 - 2.4 \text{ keV}$ luminosities and radii typically in the range $10^{34} - 10^{36} \text{ erg s}^{-1}$ and $10 - 30 \text{ pc}$ for remnants with soft thermal spectra (e.g. Smith et al. 1994; Rho 1996). If any of the components seen by the HRI are supernova remnants then they would be, by definition, the most luminous SNR in NGC 5253, and hence not typical. A more informative comparison is with the most luminous thermal X-ray emitting remnants in the LMC: N123D, N63A & N49 (Hughes, Hayashi & Koyama 1998). These have $0.5 - 4.0 \text{ keV}$ luminosities of $3, 2$ and $0.6 \times 10^{37} \text{ erg s}^{-1}$ respectively (luminosities for the observed HRI components in the equivalent band are $\sim 60\%$ of their $0.1 - 2.4 \text{ keV}$ luminosities). These middle aged ($4 - 6 \times 10^3 \text{ yr}$) X-ray luminous remnants have radii on the low end of the range quoted above, e.g. $R \approx 8 \text{ pc}$ for N49 to $R \approx 12 \text{ pc}$ for N132D. The inferred ambient ISM densities for these three SNR, between $2 - 4 \text{ H cm}^{-3}$, are the highest of Hughes et al.'s (1998) sample of the seven brightest thermal X-ray emitting SNRs in the LMC.

With an estimated SN rate of 10^{-3} yr^{-1} for the starburst in NGC 5253, one or more of the observed components could be luminous, middle aged ($\sim 5000 \text{ yr}$) SNRs similar to those seen in the LMC if the ambient density in their vicinity was reasonably high. A wide range of observations

(H α : Martin 1997, CO: Turner, Beck & Hurt 1997, strong and patchy absorption and dust lanes: Calzetti et al. 1997) demonstrate the presence of dense gas in the starburst region. The main problem with individual luminous SNRs being the source of the components seen by the HRI is trying to explain the extended components. The luminous SNRs in the LMC are significantly smaller ($R_{\text{SNR}} \sim 10 \text{ pc}$) than the estimated sizes for the extended components (HWHM in the range ~ 30 to $\sim 80 \text{ pc}$). A lower ambient density can give larger remnants, but also reduces their X-ray luminosity. One solution is to argue that the measured extension is a consequence of multiple sources within a similarly sized region, in which their sizes and individual luminosities can be smaller. This model, while a possibility, is beginning to require a number of reasonably luminous thermal X-ray emitting SNRs that may be unrealistic given the observed limits of $\lesssim 10$ SNRs based on the radio spectrum and the SN rate estimated above, if we are to explain all the apparently extended X-ray components as supernova remnants.

5.5 Superbubbles

Superbubbles are pressure driven bubbles in the ISM, inflated by the combined mechanical energy input from stellar winds and SNe from the population massive stars within them. We refer the reader to the extensive literature on the subject for a more detailed background (see McCray & Kafatos 1987; Mac Low & McCray 1988; Tenorio-Tagle & Bodenheimer 1988; Mac Low, McCray & Norman 1989; Chu & Mac Low 1990; Wang & Helfand 1991; Shull & Saken 1995 among others).

Fig. 5 shows an idealised model for the structure of a superbubble. A population of massive stars inject kinetic energy and mass from stellar winds and SNe in the central star cluster. It is assumed that shocks efficiently thermalise this energy, creating a very hot, high pressure reservoir of gas ($T \sim 10^8 \text{ K}$ for typical values of L_w and \dot{M}_w , assuming no significant initial radiative energy losses and no additional mass loading from clouds). This drives an outflow that becomes supersonic outside the mass and energy injection region. The structure of the central region and the free wind are given analytically by Chevalier & Clegg (1985). The freely expanding wind is surrounded by a region of hot, shocked wind, which occupies the majority of the volume of the superbubble. The bubble interior is the source of the X-ray emission from the superbubble. A contact discontinuity separates the hot bubble interior from a shell of swept-up and shocked ISM. The cooling time of this shell is typically short compared to the expansion time scale of the bubble, leading to a cool, $T \sim 10^4 \text{ K}$, dense shell. The outer edge of the shell is a shock wave propagating into the undisturbed ISM surrounding the bubble.

In this simple description, all the mass in the hot bubble interior is supplied from the mass loss from the central star cluster, and all the mass of the swept up ISM is confined to the cool shell. In practice, additional mass enters the hot shocked wind, enhancing its density and cooling the interior. In the absence of magnetic fields, thermal electrons from the hot interior cross the contact discontinuity and heat the edge of the cold shell. This thermal conduction leads to the evaporation of a small fraction of the cold shell mass into the bubble's interior, which can significantly enhance the

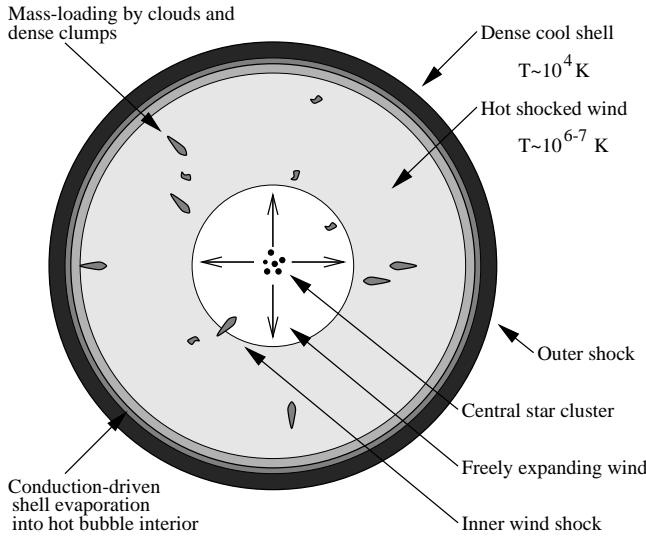


Figure 5. A schematic picture of a superbubble.

density within the bubble interior. Another source of mass for the bubble interior is hydrodynamical ablation and destruction (“mass-loading”) of dense interstellar clumps and clouds that have been overrun by the bubble (see Hartquist et al. 1986; Klein, McKee & Colella 1994; Arthur, Dyson & Hartquist 1993 and references therein), or their evaporation due to thermal conduction (Cowie & McKee 1977). Sources of additional mass in the hot bubble are of particular importance when considering the X-ray emission from superbubbles, as X-ray emission is a two body process, and the luminosity depends on the density squared.

Superbubbles are physically very similar to wind-blown bubbles around individual massive stars, apart from the slightly different mechanism of mass and energy injection. The models of Castor et al. (1975) and Weaver et al. (1977; henceforth called the Weaver model) for such bubbles around single massive stars form the basis for the analytical treatment of superbubbles, and are commonly applied directly to superbubbles without any modification.

The Weaver model is a one-dimensional similarity solution for the structure and evolution of a wind-blown bubble of *constant* mass and energy injection, expanding into a homogeneous ISM of uniform density. The solution applies for times when radiative cooling of the tenuous, hot interior of the bubble is negligible, but once the swept up ISM has cooled and collapsed to form a thin, cool ($T \sim 10^4$ K) shell. The Weaver model incorporates thermal conduction between the hot ($T \sim 10^7$ K) bubble interior and the cold shell, leading to evaporation of material off the shell, cooling and enhancing the density within the bubble interior. For convenience we reproduce two relationships for the radius of the contact discontinuity (Castor et al. 1975),

$$R_c = 0.76 (L_w / \rho_0)^{1/5} t^{3/5}, \quad (1)$$

and the X-ray luminosity, incorporating the effects of conduction (Chu & Mac Low 1990),

$$L_X \propto \Lambda_X(T, Z) \rho_0^{17/35} L_w^{33/35} t^{19/35}. \quad (2)$$

L_w is the mechanical energy injection rate due to SNe and stellar winds, ρ_0 the ambient density, t the age of the bubble and $\Lambda_X(T, Z)$ the X-ray emissivity, which is a function of temperature T and metallicity Z .

The Weaver model has widely been used in interpreting the X-ray emission from wind-blown bubbles and superbubbles in the Galaxy (e.g. Wrigge, Wendker & Wisotzki 1994), and extragalactic bubbles (Martin & Kennicutt 1995; Heckman et al. 1995; Stevens & Strickland 1998a), in particular in the LMC (Chu & Mac Low 1990; Wang & Helfand 1991; Oey & Massey 1995).

The main limitation of the Weaver model is its assumption of a constant energy injection rate, and a single phase, uniform density ambient medium, neither of which apply in reality. As can be seen from Fig. 6a, the mechanical energy injection rate from a young, co-eval population of massive stars is a strongly varying function of time. This, as we shall show below, has a strong effect on the soft X-ray luminosity as a function of time.

A variety of techniques have been developed to explore more complex situations than the standard Weaver model allows:

(i) **Analytical models:** Several workers (e.g. Koo & McKee 1992; Ostriker & McKee 1988; Zhekov & Perinotto 1996) have extended Weaver et al.’s (1977) similarity solution from uniform density and energy injection rates to power law density distributions and energy injection rates. These solutions can even incorporate conduction (Zhekov & Perinotto 1996), assuming that the time-scale for the bubble to come into conductive equilibrium is short compared to the expansion time-scale.

For our purposes these solutions are less than ideal, as the time-dependent mass and energy injection from a young cluster in a starburst region is not well approximated by a power law in time (Fig. 6a). Analytical models also fail to incorporate the hydrodynamical instabilities that can be crucial in shaping the dynamics and properties of these bubbles (see the hydrodynamic simulations of wind-blown bubbles by García-Segura, Mac Low & Langer 1996).

(ii) **Semi-analytic numerical models:** If only the bubble’s radius and velocity are required, an elegant solution not requiring detailed numerical hydrodynamics, and one that can be used for a wider range of density distributions and energy injection rates, is to use the Kompaneets thin-shell approximation (see Mac Low & McCray 1988; Shull & Saken 1995; Oey & Massey 1995). This does not provide any information regarding the bubble interior other than its pressure, and hence can not be used to explore its X-ray properties.

An approximation employed by Mac Low & McCray (1988) and Chu & Mac Low (1990) is to assume that as each instant the radial density and temperature within the bubble obey the steady-state conduction dominated similarity solution of Weaver et al. (1977):

$$T(r) = T_{\text{cen}} (1 - r/R_c)^{2/5}, \quad (3)$$

$$n(r) = n_{\text{cen}} (1 - r/R_c)^{-2/5}, \quad (4)$$

where T_{cen} and n_{cen} are the central temperature and density of the bubble respectively. The internal structure of the bubble, and hence the X-ray emission, can be calculated at each instant in such a semi-analytical model as T_{cen} is a simple function of the current bubble pressure p ,

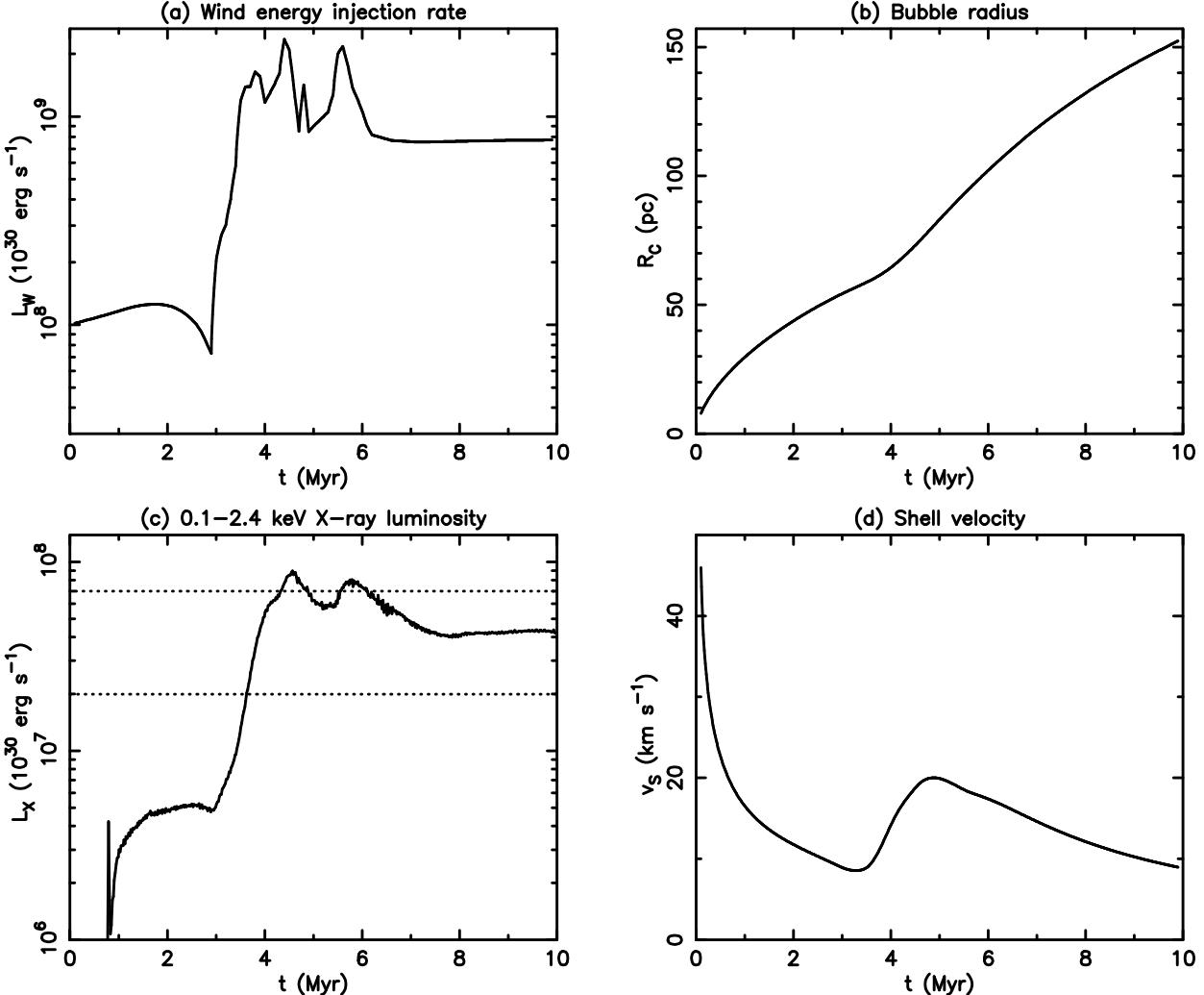


Figure 6. Properties of a superbubble blown by a cluster of total mass between $0.1 - 100 M_\odot$ of $10^5 M_\odot$. (a) Mechanical energy injection rate L_w as a function of time, from Leitherer & Heckman's (1995) starburst models, assuming an instantaneous burst, a Salpeter IMF and a metal abundance of 0.25 Solar. (b) Radius of the contact discontinuity separating the hot bubble from the cool shell of swept up ISM, as a function of time. This is the radius to which X-ray emitting gas extends. (c) X-ray luminosity as a function of time in the *ROSAT* 0.1 – 2.4 keV band from the hydrodynamic simulation described in § 5.5.2. Note the similarity in shape to the mechanical energy injection rate L_w . The dashed lines show the range of X-ray luminosities inferred for the individual X-ray components given in Table 1. (d) Shell velocity v_s . The shell is Rayleigh-Taylor unstable between $t \approx 3.5$ and 5 Myr as it is accelerated by the sudden increase in pressure in the bubble interior from the first SNe.

age t , radius R_c , and the coefficient of classical conductivity $C \approx 6 \times 10^{-7}$ erg s $^{-1}$ cm $^{-1}$ K $^{-7/2}$ (Cowie & McKee 1977):

$$T_{\text{cen}} = A \left(\frac{p R_c^2}{t C} \right)^{2/7}. \quad (5)$$

The numerical constant $A = 1.646$ is taken from Weaver et al. (1977). Again this method assumes that the bubble rapidly comes into conductive equilibrium.

These semi-analytical methods are more flexible than the purely analytical models described in (i) above, and can even be used when the density distribution is not spherically symmetric, but again do not incorporate important features such as hydrodynamical instabilities.

(iii) Computational hydrodynamical models: Although computationally far more expensive than the two methods described above, numerical hydrodynamical models are much more flexible. Gravity, radiative cooling, instabilities,

time-varying energy injection, and complex density distributions can all be included.

Their main disadvantages are their computational cost, limited physics (*e.g.* typically conduction is not included in multidimensional hydrodynamic codes), and finite numerical resolution.

We have chosen to investigate the evolution young superbubble blown by a super star cluster, with time varying mass and energy injection using the 2-D hydrodynamic code VH-1. VH-1 is a third order scheme based on the Piecewise Parabolic Method of Colella & Woodward (1984), with excellent shock handling and low numerical diffusion characteristics. See Strickland & Stevens (1998) for more discussion regarding VH-1, and X-ray emission from wind-blown bubbles.

The simulations described in this paper only investigate a relatively simple model (see § 5.5.2), of a single su-

perbubble evolving into a constant density medium. Hence the semi-analytical models described above can be used to provide an important independent check on the results of the hydrodynamical simulations, and to quantify the effect of thermal conduction, which VH-1 does not include (see § 5.5.4). This semi-analytical method was used to produce Figs. 6b & d (bubble radius and shell velocity as a function of time), given the same model parameters as used in the hydrodynamic simulation described in § 5.5.2. Future work on more complex hydrodynamical situations, for example the interaction and evolution of multiple superbubbles, can only be done with multidimensional numerical hydrodynamics.

5.5.1 Bubbles blown by individual clusters

The standard picture of starburst driven superbubbles and galactic winds is that energy and mass injection over a starburst region, typically several hundred parsecs in size, is efficiently thermalised, creating a hot central region out of which the hot gas expands and accelerates, as depicted in Fig. 5. This is based on Chevalier & Clegg's (1985) model for spherically symmetric galactic winds, since used widely in theoretical (e.g. Heckman, Armus & Miley 1990) and hydrodynamical (e.g. Tomisaka & Ikeuchi 1988; Tomisaka & Bregman 1993; Suchkov et al. 1994) work. Chevalier & Clegg assumed the mass and energy injection was uniformly distributed over the starburst region. Observationally we know a significant fraction of the massive stars in starburst regions are associated with associations and compact clusters. Meurer et al. (1995) estimate $\sim 20\%$ of the 2200 Å light in NGC 5253 comes from the clusters. As a result the mass and energy injection rate per unit volume will vary strongly within the starburst region.

We can estimate the injection rates over the entire starburst region from § 5.4. Ignoring stellar winds, then the average energy injection rate per unit volume Q_E is simply related to the SN rate N_{SN} and the radius of the region considered, by $Q_E = 3 N_{\text{SN}} / 4\pi R^3$.

For the entire starburst region, $Q_E \approx 2 \times 10^{-10}$ SN $\text{yr}^{-1} \text{pc}^{-3}$, where we have taken the total SN rate to be $N_{\text{SN}} = 10^{-3} \text{ yr}^{-1}$ from § 5.4 and used the effective radius of the starburst region of 100 pc from Meurer et al. (1995). The true volume of massive star formation within NGC 5253 is quite a bit larger than the effective radius used above, as can be seen from Fig. 2, where it covers a projected area of ~ 400 pc square, so Q_E may be an order of magnitude lower.

We can use the observed sizes and masses/stellar populations of the SSCs from the HST imaging observations of Meurer et al. (1995), Gorjian (1996) and Calzetti et al. (1997) and the long-slit spectroscopic work of Schaefer et al. (1997) (summarised in Table 2) to estimate the SN rate in individual young clusters.

A cluster of total mass of $10^5 M_\odot$, assuming a Salpeter IMF extending between $0.1 - 100 M_\odot$, has a roughly constant SN rate $N_{\text{SN}} \sim 4 \times 10^{-5} \text{ yr}^{-1}$ between the ages of $3.5 - 30$ Myr and an effective radius $R \sim 3$ pc. Hence $Q_E \approx 4 \times 10^{-7} \text{ SN yr}^{-1} \text{ pc}^{-3}$, several orders of magnitude higher than the average energy injection rate over the entire starburst region.

Similarly the mass injection rates into the clusters will be several orders of magnitude greater than the average mass

injection rate into the entire starburst region, and the resulting gas pressure will be similarly greater. As a result individual clusters should blow strong winds into the surrounding regions of the starburst, even if the entire starburst region is within a single superbubble cavity.

Depending on the separation between individual massive clusters, and the history of star formation in the vicinity, there may or may not be periods during which each cluster blows its own superbubble before bubbles meet and merge.

5.5.2 Superbubble simulation

The purpose of this simulation is to obtain an order-of-magnitude estimate of the X-ray luminosity of a young superbubble as a function of time. Given the uncertainty in the masses and ages of the clusters in NGC 5253, and the state of the (multi-phase) ISM, a detailed comparison of the observed X-ray emission with hydrodynamical modeling requires exploring a large parameter space. As discussed below in § 5.5.4, there are several factors that can alter the X-ray luminosities inferred from the HRI observation and those from our simulations. We therefore feel it sensible to proceed in a stage-by-stage basis, first establishing if a simple model can provide approximately the correct X-ray luminosity, and leaving more a detailed modeling study of young superbubbles, including additional physics such as a non-uniform ISM and mass loading by clouds, to a later date.

We simulated the first 10 Myr of the evolution of a bubble blown by a cluster of stars of total mass $M_* = 10^5 M_\odot$, assuming a Salpeter IMF extending between $0.1 - 100 M_\odot$. This mass is typical of the estimated masses for several of the brightest clusters in NGC 5253 (see Table 2). We assume all the stars within the cluster form at the same time, and scale the masses and energy injection rates for quarter Solar abundance from LH95 down to this mass. The ISM is assumed to be ionised, uniform and stationary over the region of interest, with an ambient number density of $n_0 = 100 \text{ cm}^{-3}$ and temperature $T_0 = 10^4 \text{ K}$. Radiative cooling for the assumed metallicity of $Z = 0.25 Z_\odot$ was incorporated using a parameterised form of the Raymond-Smith emissivities that can be scaled to a chosen metallicity. A minimum temperature of 10^4 K was imposed to prevent over-cooling, and to represent heating of the gas by the strong radiation field from the massive stars in the starburst region. Gravitational and magnetic forces were assumed to be negligible in comparison to the purely hydrodynamical forces at work. Mass and energy were injected with each computational time step within the radius of cluster, $R_* = 1.3 \times 10^{19} \text{ cm} \approx 4.2 \text{ pc}$. The computational grid comprised 225×225 uniformly sized zones, covering a physical region $4.5 \times 10^{20} \text{ cm} \approx 146 \text{ pc}$ square, and run in cylindrical coordinates assuming rotational symmetry around the x-axis.

In addition to this baseline simulation we describe, we performed two other simulations. To investigate how our results depend on numerical resolution we ran a simulation with the same model parameters at the basic model, except computational cells half the size and only covering $2.8 \times 10^{20} \text{ cm} \approx 90 \text{ pc}$ square. This allows to quantify the effects of numerical resolution on the derived X-ray luminosities (see § 5.5.4). To study how the wind mechanical luminosity L_w affects the X-ray emission we ran a simulation with a more massive star cluster, $M_* = 10^6 M_\odot$, with otherwise

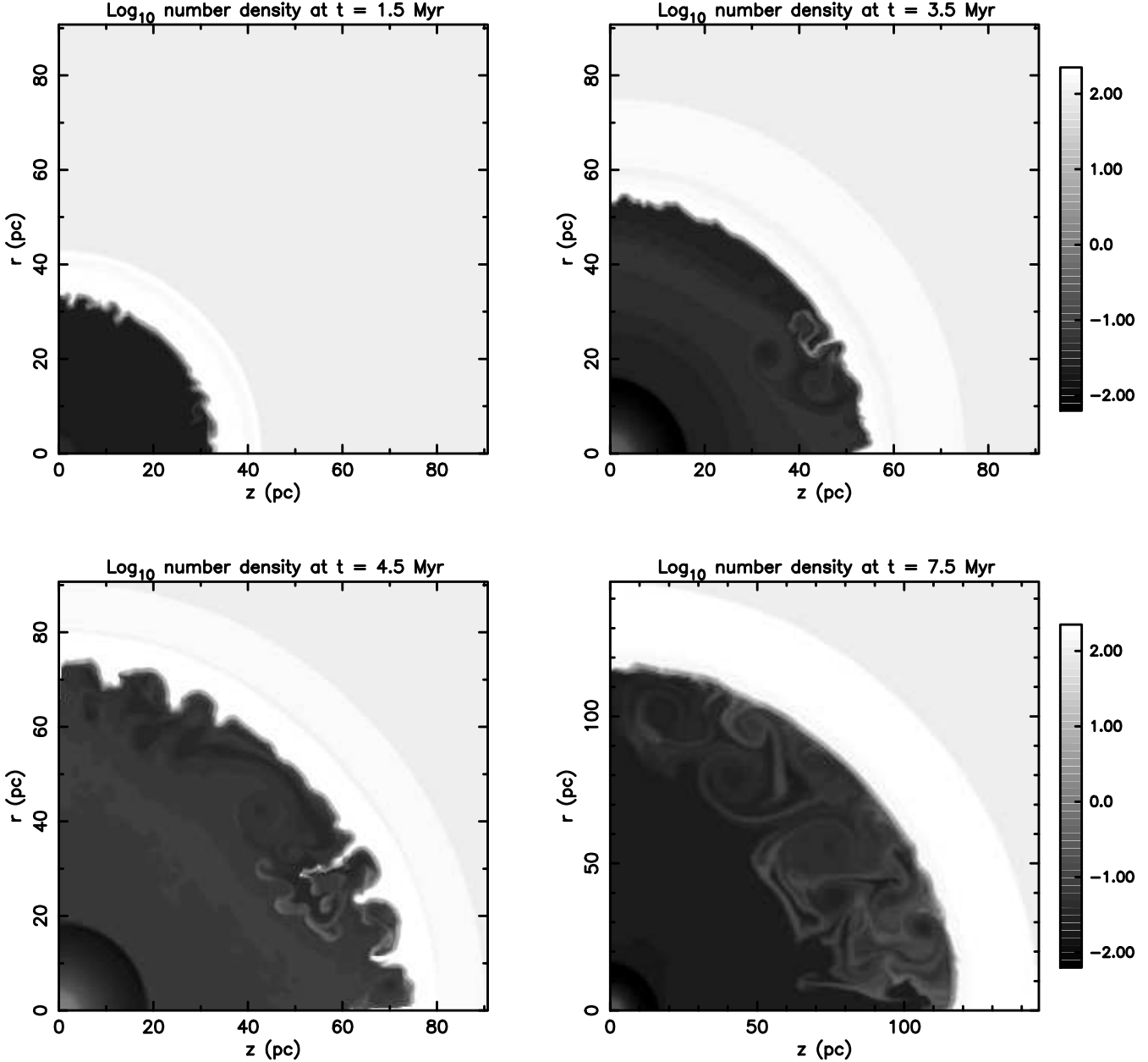


Figure 7. Superbubble density structure at four epochs representative of the structure during the initial 10 Myr, for the simulation described in Section 5.5.2. The bubble structure at $t = 1.5$ Myr is typical of the first 3 Myr, when the mass and energy injection is supplied by stellar winds only, and the hot bubble interior and cold shell are quite distinct. The additional thermal energy in the bubble interior from the first SNe occurring at $t \gtrsim 3$ Myr compresses and accelerates the superbubble shell outwards between $t \approx 3.5 - 4$ Myr. The early stages of the resulting Rayleigh-Taylor (R-T) instability in the shell can be seen at $t = 3.5$ Myr, while at $t = 4.5$ Myr the instability is at its most developed stage. After $t \approx 4$ Myr the shell is once again R-T stable, and the existing R-T ‘fingers’ are slowly destroyed and mixed into the hot interior by turbulent motions within the bubble. By $t = 7.5$ Myr the shell is smooth and only regions of enhanced density remain within the bubble interior.

the same model parameters as the first simulation. Both of these secondary simulations evolve off their computational grids at $t \sim 5$ Myr.

Note that we assume a high ambient number density $n_0 = 100 \text{ cm}^{-3}$. The resulting ISM pressure of $P/k = 10^6 \text{ K cm}^{-3}$ is much higher than the typical pressure of the undisturbed ISM in the Galaxy, $P/k \sim 3000 \text{ K cm}^{-3}$, but pressure within starburst regions is known to be significantly

higher than in the normal ISM (see Heckman et al. 1990). This value of n_0 was chosen as much for computational reasons, as discussed below, as for scientific reasons. High density gas from the parent molecular cloud undoubtedly surrounds young clusters, although its structure is very complex as can be seen in local star forming regions such as Orion.

We can crudely estimate the average ISM conditions in the center of NGC 5253 from the literature: Kobulnicky

& Skillman (1995) report a peak beamed averaged HI column density of $2.6 \times 10^{21} \text{ cm}^{-2}$ towards the core. If we assume a filling factor of unity and a path length similar to the beam size of $l = 1 \text{ kpc}$, then the volume averaged $n_{\text{H}} \approx N_{\text{H}}/l \sim 1 \text{ cm}^{-3}$. Martin (1997) estimates the electron density in warm photoionised gas at the centre of NGC 5253 to be $n_e = 246^{+49}_{-6} \text{ cm}^{-3}$, from optical spectroscopy and imaging, with a filling factor of ≈ 0.01 . This does provide evidence of a high thermal pressure in the warm phase of NGC 5253's ISM. Similarly high ambient densities and pressure have been inferred from observations of the 30 Doradus giant HII region in the LMC (see §. 5.6).

This simulation is computationally challenging to run on a workstation. The problem is following the evolution of the superbubble for 10 Myr, given the characteristic sizes and time-scales involved. The computational time step is determined by the Courant condition, $dt = C \times dx / \max(v, c_s)$, where $C = 0.5$ is the Courant number, dx is the cell size and $\max(v, c_s)$ is the maximum velocity or sound speed on the grid. For much of the simulation the sound speed within the energy injection region $c_s \sim 1500 \text{ km s}^{-1}$ is the maximum velocity. The typical size of the energy injection region is a few parsecs, given that the half-light radii of the observed clusters are $\sim 3 \text{ pc}$, and this radius must be covered by several ($\gtrsim 6$) computational cells to give a reasonable approximation to a spherical cluster. For the computational grid used above, $dt \approx 210 \text{ yr}$, hence we require $\sim 5 \times 10^4$ computational time steps to cover 10 Myr. To keep the runtime to a sensible level, even on a fast workstation, requires using as small a number of cells as possible. As the radius of the contact discontinuity $R_c \propto n_0^{-1/5}$ for fixed t and L_w , increasing the ambient density results in a smaller superbubble and hence less cells are required in the simulation.

An alternative solution to this problem used by Mac Low et al. (1989; Mac Low & Ferrara 1998) is to artificially reduce the maximum velocity on the grid by increasing the mass injection rate by some factor while keeping the energy injection rate constant. This increases dt , and lowers the number of computational steps required. It can also be used to roughly approximate the effect of conduction in increasing the density of the bubble interior. We chose not to use this approach, as the density structure of the bubble interior with conduction is not known for time varying energy injection rates, and it will strongly affect the X-ray luminosity due to the density squared dependence of L_X . Conduction-driven evaporation off the cold shell is an outside-inwards process, and it is not immediately apparent if Mac Low et al.'s method of additional mass injection inside-outwards is a reasonable substitute.

For the first 3 Myr the energy injection rate into the superbubble is approximately constant at $L_w \approx 10^{38} \text{ erg s}^{-1}$. The radius of the contact discontinuity R_c and the velocity of the shell agree well with the thin-shell solutions shown in Fig. 6.

The shell of swept-up ISM is well resolved in our simulations, and is relatively thick. Densities in the shell are only a few times that of the ambient ISM, due to the low Mach number \mathcal{M} of the forward shock. This is a consequence of our high chosen value for the ambient number density n_0 , as $\mathcal{M} \propto n_0^{-1/5}$.

Between $t = 3$ and 7 Myr the most massive O stars evolve off the main sequence and pass through a Wolf-Rayet

phase, before going SN. Note that both clusters G1 and G2 are currently in this WR phase (Schaerer et al. 1997). The first SNe very rapidly increase the wind luminosity to $L_w \approx 10^{39} \text{ erg s}^{-1}$. The increase in energy injection is matched by an almost equal increase in the mass injection rate, with the result that the temperature of the bubble interior does not change significantly.

The sudden increase in thermal pressure of the hot bubble from $t = 3 \text{ Myr}$ accelerates and compresses the shell. (Fig. 6d & 7). The acceleration of the shell causes it to become Rayleigh-Taylor (R-T) unstable between $t \sim 3.5$ and 4 Myr, and R-T fingers of cool shell material penetrate the hot bubble before being mixed in and destroyed. Note that the growth rate of the R-T instability is inversely proportional to the square root of the shell thickness (c.f. Tenorio-Tagle et al. 1997), so that for lower ambient density n_0 more shell material will enter the bubble interior, which may increase the X-ray emission as discussed below.

After $t = 5 \text{ Myr}$ the shell is decelerating once more, and is R-T stable. The R-T fingers are mixed into the bubble interior by a system of swirling, turbulent motions initiated by the interaction between the corrugations in the bubble-shell interface and the slightly faster moving (than the shell) bubble interior (Fig. 7).

5.5.3 X-ray emission as a function of time

We calculated the X-ray emission from the bubble in the *ROSAT* band within the hydro-code itself using a parameterised form of the Raymond-Smith 0.1 – 2.4 keV X-ray emissivities that can be scaled with metallicity, accurate to within a few percent. For each cell the product of $n_e n_{\text{H}} \Lambda_X(T, Z)$ was calculated, and multiplied by the volume of each cell using the rotational symmetry around the x-axis. The sum over the entire computational grid gives the estimated X-ray luminosity, as shown in Fig. 6c.

Comparing the mechanical energy injection rate with the X-ray emission in the *ROSAT* band (Fig. 6a & c), it is clear that they are very similar in shape, although there is a slight time lag between changes in L_w and a corresponding alteration in L_X . $L_X(t)$ shows the same dramatic increase at $t \sim 3 \text{ Myr}$ as the energy injection rate does, peaking at $L_X \approx 9 \times 10^{37} \text{ erg s}^{-1}$, and settling down to a constant $4 \times 10^{37} \text{ erg s}^{-1}$ after $t = 8 \text{ Myr}$. The X-ray luminosity is at its maximum during the Wolf-Rayet phase between 3 and 7 Myr. The superbubble converts a few percent, $L_X(t) \approx 0.05 \times L_w$, of the input mechanical luminosity into soft X-ray emission.

These X-ray luminosities are remarkably similar to those inferred for the marginally extended X-ray sources seen by the HRI in NGC 5253 ($L_X \approx 2 - 7 \times 10^{37} \text{ erg s}^{-1}$). This is probably a coincidence, as there are a variety of factors that can alter the X-ray luminosity of the superbubble, and the values inferred from X-ray observations.

5.5.4 Factors affecting L_X

The X-ray luminosities derived in our simulations depend on the model parameters and the physics used. The X-ray luminosities derived from our HRI data and other worker's observations also suffer from a major systematic source of

uncertainty not reflected by the statistical errors (see Strickland & Stevens 1998). Although difficult to quantify, it is worth discussing these uncertainties and how they might alter both the simulated and observed X-ray luminosities.

Conduction: Our code does not include the effects of conduction-driven evaporation off the cold shell into the hot bubble. Conduction will increase the soft X-ray luminosity of young superbubbles, as the density inside the hot shocked wind is increased by mass from the shell entering and cooling the bubble interior from a few $\times 10^7$ K to a few $\times 10^6$ K. Note that the X-ray emissivity within the *ROSAT* band peaks at $\sim 10^{6.8}$ K, so part of the luminosity increase will come from increased X-ray emissivity, although the major effect is due to increasing the number density of the X-ray emitting gas as $L_X \propto n_e^2$.

Using the semi-analytical method described in § 5.5 we find the *ROSAT*-band X-ray emission in a conduction-dominated superbubble is very similar in form to that found in our hydrodynamical simulations, although always more luminous. The 0.1–2.4 keV luminosity peaks at exactly the same time as in our simulations, with $L_X = 2 \times 10^{38}$ erg s $^{-1}$. At later times, for $t \geq 7$ Myr, the X-ray luminosity $L_X \approx 1.3 \times 10^{38}$ erg s $^{-1}$ is approximately constant.

In general this simple conductive model (which does not incorporate hydrodynamical instabilities such the R-T instability, which will increase the X-ray luminosity through the introduction of more mass into the interior and an increased conduction evaporation rate) the X-ray luminosities are typically between 2–4 times that in our hydrodynamical simulation.

Numerical resolution and diffusion: With hydrodynamical models it is always important to investigate how the results depend on the numerical resolution of the simulation. In models of superbubbles numerical diffusion can lead to unphysically large amounts of shell material entering the hot bubble interior, and hence giving unphysically high luminosities.

We could only follow our higher resolution simulation until $t = 5$ Myr, but the qualitative structure and behaviour of the superbubble during this period were very similar to the default lower resolution simulation that we have described in detail. The general features of these simulations are therefore not strongly affected by the numerical resolution.

The 0.1–2.4 keV X-ray luminosities in the higher resolution simulation were typically only $\sim 60\%$ of those in the default simulation. This indicates that the structure of the default bubble is not fully resolved. The simulation is not so under-resolved as to be unphysical, as the derived X-ray luminosities are always lower than those derived from the conductive semi-analytical model mentioned above.

Mass-loading: Hydrodynamical ablation and destruction of dense clouds overrun by the bubble will also increase the X-ray luminosity by increasing the density within the bubble interior, although the magnitude of this effect requires investigation. Large amounts of dense molecular gas left over from the parent molecular cloud can be seen in young Galactic star formation regions, *e.g.* Orion (see Wiesemann & Ho 1996 and references therein). Radio observations of the classic starburst galaxy M82 suggests the presence of clumpy, high density clouds (*e.g.* Allen & Kronberg 1998) within the starburst region. Mass-loading is believed to be

important in understanding the X-ray luminosity of SN remnants in the LMC (*e.g.* Arthur et al. 1993).

Cluster mass: The energy injection rate L_w (and hence L_X) scales linearly with the mass of the star cluster. From Table 2 it is clear that there is some uncertainty in the cluster masses, mainly due to different assumptions concerning cluster ages and optical extinction. For example, Meurer et al. (1995) assume all the clusters suffer 1.52 magnitudes of extinction at $\lambda = 220$ nm, and are at their peak UV brightness. Calzetti et al. (1997), in a multi-wavelength HST study, find very patchy extinction, reaching $A_V = 9 - 35$ magnitudes towards the brightest cluster G1.

Compared to our basic model of a $10^5 M_\odot$ cluster, a pessimistic view would be that the individual cluster masses may be up an order of magnitude higher or lower than that used.

Based on the comparison between the $M_\star = 10^5 M_\odot$ cluster and the $10^6 M_\odot$ simulation the X-ray luminosity is almost directly proportional to L_w , and hence the cluster mass, $L_X \propto M_\star$. Experiments with the semi-analytical conductive bubble model confirm that the X-ray luminosity is almost directly proportional to L_w and hence M_\star .

More X-ray luminous superbubbles can be obtained simply by increasing the mass of the star cluster, but bear in mind that the X-ray observations also place limits on the size of these putative superbubbles, and the size depends on the energy injection rate $R \propto L_w^{1/5}$.

Cluster ages: Our simulations only cover the first 10 Myr, before the shell evolves off the computational grid, so the X-ray luminosities for older bubbles are uncertain. The energy injection rate remains almost constant until an age of ~ 30 Myr before declining as the least massive stars that undergo core collapse die. The major effect that will affect L_X after $t = 10$ Myr will be changing ambient density, as the bubble expands, and potentially interacts with other bubbles and cavities in the ISM.

The ages for clusters G4 & G5 of ~ 50 Myr derived by Calzetti et al. (1997) are problematic for explaining HRI component E by a superbubble. Assuming n_0 and L_w remain constant, the radius of a 50 Myr old superbubble is 2.6 times that of a 10 Myr old bubble, *i.e.* ~ 400 pc for the parameters used in the hydrodynamic simulation. A bubble this large would subtend $20''$ on the sky at the distance of NGC 5253, much larger than component E! Lower cluster masses and hence lower energy injection rates cannot be used to avoid this problem, as $L_X \propto L_w$, and the bubble radius is less sensitive to changes in L_w or n_0 than changes in age (Eqn. 1).

We speculate that the ages inferred for these clusters have been over-estimated. For clusters G1 & G2 Calzetti et al. use H α and H β equivalent widths to estimate the cluster ages, which agree well with those derived in Schaerer et al.'s (1997) spectroscopic study. For the other clusters Calzetti et al. use colours to estimate the age. Such colour-based age diagnostics do become less sensitive with increasing age, as shown in their Fig. 8. Spectroscopic observations, which have been shown to be of great use in explaining the complex star formation history of the SSCs in NGC 1569 (González Delgado et al. 1997), have yet to be done on all the clusters in NGC 5253. This would be of great use in determining the star formation history of such an important starburst galaxy.

Ambient Density: We used a high ambient density of $n_0 = 100 \text{ cm}^{-3}$. From the standard Weaver model, $L_X \propto n_0^{17/35}$, so for an ambient density of 1 cm^{-3} , the X-ray luminosity will be approximately an order of magnitude lower than our simulation.

Note that for lower n_0 the shell is more R-T unstable, as the shell will be thinner and the growth time for the R-T instability is proportional to the square root of the shell thickness. This should introduce more mass into the bubble interior, which should act to increase the soft X-ray luminosity to some degree, *e.g.* by enhanced conductive evaporation into the hot interior from R-T fingers penetrating into the bubble.

Metallicity: SN ejecta and stellar winds from the evolved massive stars will enrich the superbubble with freshly synthesised heavy elements. Conduction and mass-loading will introduce ambient, *i.e.* less processed, less enriched material, reducing the metallicity of the X-ray emitting gas. An exact calculation of the metal abundances is outside the scope of this work, but we assumed a metal abundance (relative to Solar) of $Z = 0.25 Z_\odot$ for the hot X-ray emitting gas, slightly higher than the value of $Z \approx 1/5 Z_\odot$ from Walsh & Roy (1989).

Line emission forms a significant part of the X-ray emissivity of a hot plasma in the *ROSAT* band. To a rough approximation $\Lambda_X(T, Z) \propto Z$, so if the metal abundance (in particular the Iron abundance for emission within the *ROSAT* band) is significantly different from $0.25 Z_\odot$ the predicted superbubble X-ray luminosity from Fig. 6c will need to be scaled appropriately.

Non-ionisation equilibrium (NIE): The Raymond-Smith emissivities (1977) used in calculating the X-ray emission and the total cooling curve used in the simulation assume the plasma is in collisional ionisation equilibrium. This state is not necessarily achieved throughout superbubbles and galactic winds.

The soft X-ray emission from a superbubble will be dominated by initially cool gas mixed into the bubble interior and heated by conduction, mass loading and instabilities. The ionisation state of this gas will lag behind its temperature rise, as discussed by Weaver et al. (1977). As a result the ions that in collisional ionisation equilibrium (CIE) contribute significantly to the X-ray emission of plasmas with $T \sim 10^6 \text{ K}$ will in practice be under-ionised. In general then the true X-ray luminosity will be less than that obtained assuming CIE.

For a suddenly heated plasma, the time required to reach ionisation equilibrium, $t_{\text{ieq}} \approx 0.03 n_e^{-1} \text{ Myr}$ (Masai 1994), which for the gas dominating the intrinsic X-ray emission in our simulations (using ionisation equilibrium emissivities) is typically $10^{-3} - 3 \times 10^{-2} \text{ Myr}$, significantly shorter than the age of the superbubble. This suggests NIE effects will not be a major effect for the soft X-ray emission in this stage of superbubble evolution.

Transient increases in L_X due to SN: SNRs expanding within the tenuous bubble will not be X-ray luminous individually due to the low density, and it is assumed that their kinetic energy is thermalised within the bubble. SN can then be treated as a continuous form of energy injection, rather than individual events, and this is the approach taken in the majority of the literature. This assumption depends on the SN blast wave being subsonic by the time it

reaches the superbubble's shell. Mac Low & McCray (1988) find that the fractional radius where a SN blast wave becomes subsonic (assuming the SN occurred at the centre of the bubble) is $r/R_c \approx 0.47(E_{\text{SN}}/U_{\text{bub}})^{1/3}$, where E_{SN} is the total SN energy, U_{bub} is the thermal energy in the superbubble and R_c the radius of the contact discontinuity at the outer edge of the hot bubble interior. Thus, by the time one or two SN have occurred within the superbubble, all further SN blast waves from the central cluster will be thermalised within the superbubble. Only SN that occur near the edge of the superbubble will not be thermalised before they strike the shell.

Off-center SN blast waves striking the shell while still supersonic, causing brief ($\lesssim 10^4 \text{ yr}$) increases in X-ray luminosity, may be required to explain some X-ray bright superbubbles around OB associations in the LMC (Chu & Mac Low 1990; Wang & Helfand 1991). Chu & Mac Low use a simple semi-analytical model to study the increase in L_X due to this process, but the maximum increase they found was $\sim 10^{36} \text{ erg s}^{-1}$, which is negligible in terms of explaining the X-ray emission from NGC 5253.

Observed X-ray luminosities: The X-ray luminosities for the five components given in Table 1 assume that the spectrum is well represented by a single temperature hot plasma model. In reality the plasma inside the bubble will be multi-phase due to density variations within the isobaric bubble interior.

As discussed in Strickland & Stevens (1998), properties inferred from simple spectral model fits to multi-temperature X-ray spectra can deviate significantly, by up to an order of magnitude, from the true properties. Although the results of the *ROSAT* PSPC spectral fitting can be considered as characterising the spectral information, the X-ray luminosities quoted in Table 1 should be considered more uncertain than the formal error estimates.

5.6 A comparison with 30 Doradus

The nearest example of a star formation event approaching the intensity of that creating the clusters in NGC 5253 is 30 Doradus in the LMC. It is interesting to compare the X-ray properties of 30 Doradus, as inferred from *ROSAT* HRI and PSPC observations, with those of the individual components in NGC 5253.

Optically, the 30 Dor (Tarantula) nebula is 300 pc in diameter (Chu & Kennicutt 1994). At the distance of NGC 5253 it would subtend $15''$ on the sky. The star formation history within the nebula is acknowledged to be complex, but the central cluster R136 is probably young, $3 - 5 \text{ Myr}$ old, with estimates of the initial mass of $\gtrsim 1.7 \times 10^4 M_\odot$ (Malumuth & Heap 1994), or $\sim 3 \times 10^4 M_\odot$, upper limit $1.5 \times 10^5 M_\odot$ (Brandl et al. 1996).

The nebula is a source of diffuse soft thermal ($kT = 0.34^{+0.07}_{-0.04} \text{ keV}$) X-ray emission that peaks in holes in the optical emission, with a total luminosity between 3 and $6 \times 10^{37} \text{ erg s}^{-1}$ (Norci & O'Gorman 1995). A nearby supernova remnant, N157B, has a X-ray luminosity of $8 \times 10^{36} \text{ erg s}^{-1}$. *ROSAT* HRI observations reveal two point sources associated with the central R 136 cluster of luminosity $L_X \sim 10^{36} \text{ erg s}^{-1}$ each, that may be high mass X-ray binary black hole candidates (Wang 1995).

On the basis of the size and velocities of individual shells

and filaments, Chu & Kennicutt (1994) derive ambient number densities in the range $n_0 \approx 5 - 70 \text{ cm}^{-3}$, or $\approx 12 \text{ cm}^{-3}$ considering the entire nebula.

5.7 Summary of discussion

To summarise, the possible sources of X-ray emission that can match the luminosities inferred from the HRI observations, and can be associated with massive stars are MXRBs, SNRs and superbubbles. We would expect all of these sources to be present in NGC 5253 at some level, given the example of 30 Doradus, but the real question is which type of source is the *dominant* X-ray emitter?

Massive X-ray binaries cannot be the predominant source, primarily for spectral reasons, as the integrated spectrum from the *ROSAT* PSPC observations is that of a soft thermal plasma, unlike the generally hard X-ray spectrum associated with MXRBs. This does not rule out one or two of the observed components, *e.g.* A & D, or some fraction of the emission from the extended components, being due to massive binaries, but summed over all the components the $0.1 - 2.4 \text{ keV}$ spectrum must be soft.

Superbubbles and SNRs can both be sources of soft thermal X-ray emission, although SNRs are generally much fainter than the sources observed in NGC 5253. For a given X-ray luminosity, SNRs will be much more compact, $R_{\text{SNR}} \sim 10 \text{ pc}$, than superbubbles $R_c \sim 50 - 150 \text{ pc}$. To explain the extended HRI components as SNR would require each of the extended components (B, C & E, HWHM $\sim 30 \text{ pc} - 80 \text{ pc}$) to be comprised of several smaller SNRs, which begins to run into problems with the SN rate and the predominantly thermal radio spectrum.

It is probably inescapable that young star clusters such as those observed by the HST blow superbubbles into the ISM of the starburst region – the main question is can they be X-ray luminous and compact enough to explain the observed X-ray components? We have performed the first hydrodynamical simulations of superbubbles blown by individual super star clusters with realistic time-varying mass and energy injection rates. The soft X-ray luminosity $L_x(t)$ of the bubble was found to be proportional to the mechanical energy injection rate $L_w(t)$, implying that superbubbles should be most X-ray luminous between $t = 3 - 7 \text{ Myr}$, the Wolf-Rayet phase of the parent cluster. The soft X-ray luminosity for a superbubble blown by a $M_* = 10^5 M_\odot$ cluster during this period and up to $t = 10 \text{ Myr}$ agrees very well with the luminosities inferred for the extended components from the HRI data, although a variety of factors not considered in our simulations can influence the absolute magnitude of the X-ray luminosity.

To achieve the required X-ray luminosities with superbubbles or SNRs requires them to be expanding into a region of higher than average density. This may also explain the lack of detected X-ray emission from some of the other bright clusters. Considering the count rates of the observed components, we would not detect sources with $L_x \lesssim 5 \times 10^{36} \text{ erg s}^{-1}$, so superbubbles with lower energy injection rates or expanding into regions of lower ambient density could easily have been missed by our *ROSAT* HRI observations.

The balance of the evidence favours superbubbles as the dominant source of the X-ray emission from NGC 5253.

Only higher resolution X-ray spectral imaging by *AXAF* can conclusively prove this to be the case, and identify the origin of the individual components.

6 IMPLICATIONS FOR MASS-LOSS FROM NGC 5253 AND OTHER DWARF STARBURST GALAXIES

What implications do these possible multiple superbubbles have on starburst-driven mass loss and metal ejection from NGC 5253? What fraction of the ISM will be blown away, and how efficiently can the heavy elements synthesised by the massive stars in the starburst escape into the IGM? The long term fate of the material blown out of galaxies in galactic winds is still uncertain, but given the low escape velocities of dwarf galaxies any hot, metal enriched, thermalised SN and stellar wind ejecta that reaches the halo is probably lost.

The existing X-ray observations of NGC 5253 can not be used to meaningfully constrain the total gas mass and thermal energy content of the hot ISM. The X-ray spectrum observed by the *ROSAT* PSPC is consistent with emission from a soft thermal plasma, but this is not enough on its own to allow us to infer the properties of what is most probably, a mix of sources. Superbubbles are theoretically expected to have complex multi-temperature X-ray spectra, which as shown in Strickland & Stevens (1998) can give misleading “derived” properties when observed with *ROSAT* and fit with simplistic single or two-temperature spectral models. A more quantitative investigation of the properties of the hot gas in NGC 5253 awaits the launch of *AXAF*, which can both determine the size of any extended sources, and be used to characterise the spectral properties of each source.

We shall instead consider qualitatively the implications of the starburst upon NGC 5253, focusing on analytical and numerical studies of the effect of starburst-driven superbubbles and winds on dwarf galaxies, *e.g.* De Young & Heckman (1994) and Mac Low & Ferrara (1998).

However, these and other related theoretical work in the literature (Chevalier & Clegg 1985; Tomisaka & Ikeuchi 1988; Tomisaka & Bregman 1993), which we shall refer to as the “standard” model, implicitly assume:

- (i) A single superbubble, driven by a single region of uniform mass and energy deposition, *i.e.* the entire starburst region as a whole drives a wind into the ISM, *e.g.* Chevalier & Clegg (1985).
- (ii) A simplified energy and mass injection history, constant with time for 40 – 50 Myr, effectively based on one single instantaneous burst of star formation, and ignoring the weaker energy injection for the first 3 Myr due to stellar winds alone.
- (iii) A single phase, previously undisturbed ISM.

Compare this to the more complex situation in NGC 5253, where we have:

- (i) A more complex SF history. Super star clusters and smaller associations are physically distributed over the starburst region, with a range of different ages (although SF within an individual cluster may be co-eval), with the possibility that the region of active SF has moved from the SW to the NW (Gorjian 1996). Each cluster is probably the

source of a strong wind of thermalised SN and stellar wind ejecta, as shown in § 5.5.2. Complex SF histories, with multiple clusters of different ages seem to reasonably common, as this situation is inferred to be the case in other famous starburst galaxies such as M82 (Satyapal et al. 1997) and NGC 1569 (Vallenari & Bomans 1996; González Delgado et al. 1997).

(ii) A multiphase ISM, with molecular clouds (Turner et al. 1997), a very prominent dust lane, regions of dense warm gas (Martin & Kennicutt 1995; Martin 1997) and holes and bubbles of hot coronal gas (this work).

We shall briefly consider the qualitative effect of this more complex situation on the mass loss and metal ejection efficiency, after considering the predictions of the standard single superbubble model.

6.1 Mass loss from galaxies in the standard superbubble model

The coupling between the energy supplied by the SNe and stellar winds from the starburst and the ISM is crucial in determining the amount of gas and metal lost from dwarf galaxies. The energy supplied by the multiple supernovae is sufficient to eject a large mass of gas from the shallow gravitational potential well of a dwarf galaxy, but this energy must be transferred from the thermal energy of the hot bubble interior to kinetic energy in bulk motions of the ambient ISM.

As a simple estimate of the power of a starburst, a starburst can accelerate a mass of gas $M_{\text{acc}} \sim 10^4 f E_{51}/v_{100}^2 M_{\odot}$ to a velocity of v_{100} , where v_{100} is the velocity in units of 100 km s^{-1} , E_{51} is the total mechanical energy injected by SNe and stellar winds in units of 10^{51} erg and f measures the coupling between the superbubble and the ISM that is swept-up. For the Weaver model, with constant energy injection in a uniform ISM, only about 20% of the total energy injected ends as the kinetic energy of the swept-up ISM, 45% is stored as thermal energy in the hot shocked wind material that makes up the bubble interior and which drives the bubble's expansion, and most of the rest is radiated from the shell. In practice $f = 0.2$ is an upper limit. A single cluster of $M_{\star} = 10^5 M_{\odot}$, typical of the brighter clusters in NGC 5253, will inject $\sim 10^{54} \text{ erg}$ of mechanical energy into the ISM over the lifetime of the lowest mass star to go SN, *i.e.* $\sim 30 \text{ Myr}$. If we adopt the total initial mass for the entire starburst from § 5.4 of $\sim 5 \times 10^6 M_{\odot}$ then $E_{51} \sim 5 \times 10^4$. NGC 5253's total mass is $\lesssim 10^9 M_{\odot}$ ($3 \times 10^8 M_{\odot}$ of which is gas, Kobulnicky & Skillman 1995), so the escape velocity is $\sim 100 \text{ km s}^{-1}$, using Eqn. 28. of Mac Low & Ferrara (1998). Hence based on the very simple energetics argument above we might expect *at maximum* $\sim 10^8 M_{\odot}$ of the ISM to be ejected from NGC 5253 over the entire history of the current starburst.

Once any superbubble breaks out of the disk into the halo, the coupling of the starburst to the remaining ISM is reduced as the bubble escapes the disk and expands preferentially into the much lower density and pressure environment of any galactic halo medium and the IGM, venting the thermal energy of the bubble interior. The hot gas previously forming the superbubble interior accelerates outwards as a galactic wind, carrying with it the fragmented remains

of part of the dense superbubble shell (between 4 – 9% of the shell mass in Mac Low et al.'s [1989] simulations of superbubbles blown by normal OB associations). The amount of energy transferred to the ISM then drops once any effective chimney to the halo is created, and hence the amount of gas ejected with the hot, unbound, wind material is also reduced.

How effectively the starburst couples with the ISM depends on the structure and distribution of the ISM in the galaxy, as well as the mechanical power of the starburst. De Young & Heckman (1994) considered analytically the effect of a superbubble of constant power, lasting for 40 Myr, expanding in an uniform density elliptical ISM for galaxies of different mass, ISM density and ellipticity.

Although their models did not include massive dark matter haloes around their galaxies, their results illuminate much of the basic physics, and are worth reiterating here. They found that thin disks, dense disks, and low total energy injection all encourage blow-out along the minor axis. Conversely, thick disks, tenuous disks and high energy injection all increase the probability of a catastrophic blow-away of the ISM. Normal massive disk galaxies are very resistant to blow-away, while low mass dwarf galaxies ($\sim 10^7 M_{\odot}$) are susceptible to having their entire ISMs blown away. Typical dwarf galaxies of $M \sim 10^9 M_{\odot}$ show a wider range of possible behaviour, dependent on the distribution of the ISM.

Mac Low & Ferrara (1998) repeated De Young & Heckman's study, this time incorporating the effects of massive dark matter haloes, in an attempt to obtain quantitative estimates for the total mass and metal ejection efficiencies for a range of dwarf galaxy gas masses and mechanical luminosities, using a 2D hydrodynamic code. Again the energy injection rate was assumed to be constant in time, lasting for 50 Myr. The maximum energy injection rate they considered was $L_{\text{w}} = 10^{39} \text{ erg s}^{-1}$, equivalent to only a single $M_{\star} = 10^5 M_{\odot}$ cluster, which is unfortunately an order of magnitude or so lower than the total energy injection rate in a starbursting dwarf like NGC 5253. They found that the total mass ejected at greater than escape velocity is $\sim 10^5 M_{\odot}$ for a galaxy with a gas mass of $M_{\text{gas}} = 10^8 M_{\odot}$, although almost all the metal enriched gas escapes. Although they did not perform a higher mechanical luminosity simulation appropriate for NGC 5253 and similar starburst galaxies, their results strongly suggest only a small fraction of the total ISM mass is lost in the wind but the majority of the newly synthesised metals are lost.

Several authors have reported simulations of the more powerful starburst in M82 (Tomisaka & Ikeuchi 1988; Tomisaka & Bregman 1993; Suchkov et al. 1994, 1997), although they do not give quantitative values for the mass ejected.

6.2 Mass loss with realistic star formation histories

Suchkov et al. (1994) do use a more realistic SF history than previously considered, using the LH95 models to give the time-dependent mass and energy injection rates due to a constant star formation rate of $2 M_{\odot} \text{ yr}^{-1}$, and they stress the importance of the starburst history in altering the dynamics of a galactic wind. They found that the weak initial mass and energy injection, due to stellar winds before any

SNe, creates a cavity in the disk without strongly affecting the disk ISM. This allowed the hot gas from the much more powerful SNe dominated phase of the starburst to escape virtually freely into the halo.

We conclude that a SF history such as NGC 5253's, with the energy injection spread out more over time due to the range in cluster ages, will reduce the total mass loss from the galaxy compared to the standard single superbubble model. Hence realistic star formation histories (and more realistic, multiphase ISM distributions) will reduce the efficiency with which starbursts can strip a galaxy of its ISM compared to the single superbubble model. Although total mass loss rates may be reduced, easier venting of the hot metal-enriched gas from the starburst into the IGM will act to increase the metal ejection efficiency.

The reason weaker mass and energy injection cause less disruption to the ISM is that the total energy per unit volume (or per unit mass) they impart to the ISM by the time the bubbles blow out is less, even though it may take longer for a weaker superbubble to blow out. Post blow-out, much of the energy injected by the starburst, including any from later more powerful star formation, is simply vented directly into the halo without interacting with the remaining ISM.

This is due to the size of a superbubble being a stronger power of time than of wind luminosity L_w , so much weaker bubbles need only be slightly older to occupy the same volume as a powerful superbubble. The total energy supplied to the ISM is roughly proportional to $L_w t$. In the Weaver model, where the ambient density and the wind luminosity are constant, then the volume of the bubble $V \propto L_w^{3/5} t^{9/5}$ and the kinetic energy of the swept-up ISM is $E_{ISM} \approx 0.2 L_w t$. For time-varying energy injection and non-uniform ambient density the standard scaling relationships do not strictly apply, and the kinetic energy of the shell is not a constant fraction of the total energy injected, but as they are approximately correct we shall use them to illustrate the point. The energy per unit volume supplied to the ISM is then $E_{ISM}/V \propto L_w^{2/5} t^{-4/5}$.

Weak superbubbles supply much less energy to the ISM than more powerful ones do, even though both blow-out after sweeping up the same mass of gas. As a result weaker bubbles accelerate the ISM to lower velocities before blowing out, and with lower ram pressure are less efficient at dragging dense gas out of the disk into the halo.

For example consider two cases where the mechanical luminosities differ by a factor of ten. If we assume blow-out occurs when any superbubble reaches some critical volume determined by the structure of the ISM only, then we can evaluate both the time taken to blow-out and the energy per unit mass supplied to the ISM in terms of the wind luminosity. To occupy the same volume, $t_1/t_2 = (L_1/L_2)^{-1/3}$, a bubble an order of magnitude weaker would only take approximately twice the time to blow out, but only supply a fifth as much energy into accelerating and disrupting the ISM.

As a result, powerful starbursts that would have sufficient energy to unbind a significant portion of the ISM of a dwarf galaxy in the absence of any other star formation, may have little effect on the ISM if preceding weaker star formation and the resulting superbubbles open up channels to the halo that efficiently vent the hot gas from the main SF.

Even if we assume no preceding weaker SF within the starburst itself, natural levels of massive star formation and type Ia SN in galaxies can increase the porosity of the ISM and lead to significant filling factors of hot, low density gas in the ISM that can act as vents for starburst-driven superbubbles (e.g. see Oey & Clarke 1997; Rosen & Bregman 1995; Rosen, Bregman & Kelson 1996).

The observational properties of the starburst will also differ from the standard single superbubble case, as the structure of the ISM the superbubbles interact with will be determined by the history of mass and energy injection. The $H\alpha$ emission, due to both photoionisation and shock heating, depends on the local SF history, as the ionising flux from young clusters is a strong function of time (decreasing rapidly after ~ 5 Myr), while bubbles both cause shock heating and allow ionising photons to propagate further out from bright UV sources (see Martin 1997 for observational evidence and a discussion of this). The X-ray luminosity of the starburst is also proportional to a weak function of the ambient density (see Eqn. 2). Hence L_X will decrease after blow-out as the galactic wind encounters only low density halo gas, and as the density of the wind material decreases as it expands into the galactic halo. The main remaining regions of X-ray emission will be in the interfaces between hot tenuous wind material and any dense gas encountered, *i.e.* near the chimney walls, shell fragments and clouds the wind shocks and ablates.

6.3 Summary of implications

The total mechanical energy released by the starburst in NGC 5253 is enough to unbind a significant fraction of its ISM, but the total mass loss depends crucially on how well this energy can be transferred from the hot gas to the ISM, before any blow-out and venting of the hot shocked gas into the halo as a galactic wind.

The SF history in NGC 5253, with multiple clusters of different ages each blowing winds and bubbles into the ISM, is more complex than the single superbubble model with a single instantaneous burst of SF. We speculate that the total mass ejected from the ISM in a situation with a SF history similar to NGC 5253's will be reduced compared to the standard single superbubble model, as the more gradual energy injection allows the hot gas created by the starburst to blow-out without transferring as much energy to the ISM. Later thermalised SNe and stellar wind ejecta is then vented easily into the halo without interacting significantly with the remaining ISM. This should also act to increase the fraction of the newly synthesised heavy elements that are lost, even though the total mass lost is reduced. It is unlikely that NGC 5253 will lose a significant fraction of its ISM to starburst-driven winds, despite this being energetically feasible.

7 CONCLUSIONS

We obtained a long *ROSAT* HRI observation of the dwarf starburst galaxy NGC 5253, with the aim of resolving the superbubble believed to be present on the basis of the *ROSAT* PSPC observation of Martin & Kennicutt (1995).

- (i) Instead of a single superbubble, HRI observations

show several, at least five, separate sources of soft, 0.1-2.4 keV, X-ray emission, associated with the massive young clusters of stars at the centre of NGC 5253. Based on the PSPC spectrum the luminosities of the five components range between $L_X \approx 2 - 7 \times 10^{37}$ erg s $^{-1}$.

(ii) Three of the components are statistically extended beyond the HRI PSF at 90% confidence, the largest having a FWHM of 8_{-4}^{+10} arcsec, equivalent to 160_{-80}^{+200} pc.

(iii) The possible sources of X-ray emission that can match the luminosities inferred from the HRI observations, and are expected to be associated with massive stars are MXRBs, SNRs and superbubbles. We would expect all of these sources to be present in NGC 5253 at some level, given the example of 30 Doradus, but which is the dominant source of soft X-ray emission?

(iv) Massive X-ray binaries cannot be the predominant source, primarily for spectral reasons as the integrated spectrum from the *ROSAT* PSPC observations is that of a soft thermal plasma, unlike the generally hard X-ray spectrum associated with MXRBs. This does not rule out one or two of the observed components, or some fraction of the emission from the extended components, being due to massive binaries, but summed over all the components the 0.1 – 2.4 keV spectrum must be soft.

(v) Explaining the extended HRI components as middle-aged X-ray luminous SNRs requires each of the extended components (B, C & E, HWHM ~ 30 pc – 80 pc) to be comprised of several smaller SNRs, as for a given X-ray luminosity, SNRs will be much more compact, $R_{\text{SNR}} \sim 10$ pc, than superbubbles $R_c \sim 50 - 150$ pc. This model of several SNRs per X-ray component begins to run into problems with the SN rate and the upper limit on the total number of SNRs being $\lesssim 10$ from the thermal radio spectrum.

(vi) We show that super star clusters and other massive clusters of stars, such as those observed by the HST in the centre of NGC 5253, individually will be the source of strong winds blowing into the ISM of the starburst region. These may be the source of *multiple* young superbubbles within the central regions of a young starburst galaxy such as NGC 5253.

(vii) We have performed the first hydrodynamical simulations of superbubbles blown by individual super star clusters with realistic time-varying mass and energy injection rates, in order to investigate whether they can be X-ray luminous enough to explain the extended soft X-ray components seen in NGC 5253. The soft X-ray luminosity $L_X(t)$ of the superbubble was found to be proportional to the mechanical energy injection rate $L_w(t)$, implying that superbubbles should be most X-ray luminous between $t = 3 - 7$ Myr, the Wolf-Rayet phase of the parent cluster. This may explain why Wolf-Rayet galaxies are observed to be X-ray overluminous compared to normal spiral and more mature starburst galaxies (see Stevens & Strickland 1998a; 1998b). The predicted soft X-ray luminosity for a superbubble blown by a $M_\star = 10^5 M_\odot$ cluster during this period and up to $t = 10$ Myr agrees very well with the luminosities inferred for the extended components from the HRI data, although a variety of factors we discuss that are not considered in our simulations can influence the absolute magnitude of the X-ray luminosity.

(viii) Achieving the required X-ray luminosities with superbubbles or SNRs requires them to be expanding into a

region of higher than average density. This may also explain the lack of detected X-ray emission from some of the other bright clusters. Given the count rates for the observed components, we would not detect sources with $L_X \lesssim 5 \times 10^{36}$ erg s $^{-1}$, so superbubbles with lower energy injection rates or expanding into regions of lower ambient density could easily have been missed by our *ROSAT* HRI observations.

(ix) In conclusion, the evidence favours several of the observed X-ray sources being young superbubbles, and that superbubbles are the dominant source of the X-ray emission from NGC 5253. Only higher resolution X-ray spectral imaging by *AXAF* can conclusively prove this to be the case, and identify the origin of the individual components. If confirmed, this is the first detection of multiple superbubbles in a starburst region.

(x) We emphasise the importance of the SF history and distribution on the amount of gas and metals ejected from starbursting dwarf galaxies, in addition to the effect of the ISM distribution that previous work had highlighted (e.g. De Young & Heckman 1994; Heckman et al. 1995).

(xi) We speculate that the total mass ejected from the ISM of a dwarf galaxy in a situation with a SF history similar to NGC 5253's will be reduced compared to the standard single superbubble model, as the more gradual energy injection allows the hot gas created by the starburst to blow-out without transferring as much energy to the ISM. Later thermalised SNe and stellar wind ejecta is then vented easily into the halo without interacting significantly with the remaining ISM. This should also increase the fraction of the newly synthesised heavy elements that are lost, even though the total mass loss is reduced. It is unlikely that NGC 5253 will eject a significant fraction of its ISM to starburst-driven winds, despite this being energetically feasible.

Acknowledgements

We would like to thank Crystal Martin and Varoujan Gorjian for supplying us with optical images of NGC 5253. We would also like to thank the following people for useful discussions and constructive criticism through various stages of this work: Crystal Martin, Sally Oey, the members of the Birmingham "Galaxies and Clusters" group and the referee Mordecai-Mark Mac Low. DKS and IRS also acknowledge the funding support of PPARC and the School of Physics & Astronomy. All calculations were carried out on the local STARLINK computing node.

This research has made use of the Leitherer & Heckman (1995) starburst evolutionary synthesis models (<http://www.stsci.edu/ftp/science/starburst/>), the NASA/IPAC Extragalactic Database (NED, operated by the Jet Propulsion Laboratory, California Institute of Technology, under contract with the National Aeronautics and Space Administration), the SIMBAD database (operated by the CDS, Strasbourg) and the HST Guide Star Catalogue (The Guide Star Catalog was produced at the Space Telescope Science Institute under U.S. Government grant. These data are based on photographic data obtained using the Oschin Schmidt Telescope on Palomar Mountain and the UK Schmidt Telescope).

REFERENCES

Allen M. L., Kronberg P. P., 1998, *ApJ*, 502, 218

Arthur S. J., Dyson J. E., Hartquist T. W., 1993, *MNRAS*, 261, 425

Beck S. C., Turner J. L., Ho P. T. P., Lacy J. H., Kelly D., 1996, *ApJ*, 457, 610

Bradamante F., Matteucci F., D'Ercole A. D., 1998, *A&A*, 337, 338

Brandl B., Sams B. J., Bertoldi F., Eckart A., Genzel R., Drapatz S., Hofmann R., Löwe M., Quirrenbach A., 1996, *ApJ*, 466, 254

Briel U. G. et al., 1994, The *ROSAT* user's handbook. Max-Planck-Institut Für Extraterrestrische Physik, München

Calzetti D., Meurer G. R., Bohlin R. C., Garnett D. R., Kinney A. L., Leitherer C., Storchi-Bergmann T., 1997, *AJ*, 114, 1834 (C97)

Cash W., 1979, *ApJ*, 228, 939

Castor J., Weaver R., McCray R., 1975, *ApJ*, 200, L107

Chevalier R. A., Clegg A. W., 1985, *Nature*, 317, 44

Chu Y.-H., Kennicutt R. C., 1994, *ApJ*, 425, 720

Chu Y.-H., Mac Low M.-M., 1990, *ApJ*, 365, 510

Colella P., Woodward P. R., 1984, *J. Comp. Phys.*, 54, 115

Conti P. S., 1991, *ApJ*, 377, 115

Cowie L. L., McKee C. F., 1977, *ApJ*, 211, 135

David L. P., Harnden Jr F. R., Kearns K. E., Zombeck M. V., 1996, The *ROSAT* High Resolution Imager (HRI) Calibration Report, U.S. *ROSAT* Science Data Center/SAO

Della Ceca R., Griffiths R. E., Heckman T. M., 1997, *ApJ*, 1997, 485, 581

Dekel A., Silk J., 1986, *ApJ*, 303, 39

De Young D. S., Heckman T. M., 1994, *ApJ*, 431, 598

Dickey J. M., Lockman F. J., 1990, *ARA&A*, 28, 215

Fabbiano G., Kim D.-W., Trinchieri G., 1992, *ApJS*, 80, 531

García-Segura G., Mac Low M.-M., Langer N., 1996 *A&A*, 305, 229

González Delgado R. M., Leitherer C., Heckman T., Cerviño M., 1997, *ApJ*, 483, 705

Gorenstein P., 1975, *ApJ*, 198, 95

Gorjian V., 1996, *AJ*, 112, 1886 (G96)

Harris D. E., Silverman J. D., Hasinger G., Lehmann I., 1998, accepted for publication in *A&AS*, astro-ph/9811121

Hartquist T. W., Dyson J. E., Pettini M., Smith L. J., 1986, *MNRAS*, 221, 715

Heckman T. M., Armus L., Miley G. K., 1990, *ApJS*, 74, 833

Heckman T. M., Dahlem M., Lehnert M. D., Fabbiano G., Gilmore D., Waller W. H., 1995, *ApJ*, 448, 98

Hughes J. P., Hayashi I., Koyama K., 1998, submitted to *ApJ*, astro-ph/9802342

Klein R., McKee C. F., Colella P., 1994, *ApJ*, 420, 213

Kobulnicky H. A., Skillman E. D., 1995, *ApJ*, 454, L121

Koo B.-C., McKee C. F., 1992, 388, 103

Leitherer C., Heckman T. M., 1995, *ApJS*, 96, 9 (LH95)

Mac Low M.-M., Ferrara A., 1998, submitted to *ApJ*, astro-ph/9801237

McCray R., Kafatos M., 1987, 317, 190

Mac Low M.-M., McCray R., 1988, *ApJ*, 324, 776

Mac Low M.-M., McCray R., Norman M. L., 1989, *ApJ*, 337, 141

Malumuth E. M., Heap S. R., 1994, *AJ*, 107, 1054

Marlowe A. T., Heckman T. M., Wyse R. F. G., Schommer R., 1995, *ApJ*, 438, 563

Marlowe A. T., Meurer G. R., Heckman T. M., Schommer R., 1997, *ApJS*, 112, 285

Martin C. L., 1996, *ApJ*, 465, 680

Martin C. L., 1997, *ApJ*, 491, 561

Martin C. L., Kennicutt R. C., 1995, *ApJ*, 447, 171

Masai K., 1994, *ApJ*, 437, 770

Meurer G. R., Heckman T. M., Leitherer C., Kinney A., Robert C., Garnett D. R., 1995, *AJ*, 110, 2665 (M95)

Motch C., Pakull M. W., Pietsch W., 1994, in: Violent Star Formation from 30 Doradus to QSO's, ed. G. Tenorio-Tagle, 208

Norci L., Oğelman H., 1995, *A&A*, 302, 879

Oey M. S., Clarke C. J., 1997, *MNRAS*, 289, 570

Oey M. S., Massey P., 1995, *ApJ*, 452, 210

Ostriker J. P., McKee C. F., 1988, *Reviews of Modern Physics*, 60, 1

Raymond J. C., Smith B. W., 1977, *ApJS*, 35, 419

Rho J., 1995, Ph.D. Thesis, University of Maryland

Rieke G. H., Lebofsky M. J., Walker C. E., 1988, *ApJ*, 325, 679

Rosen A., Bregman J. N., 1995, *ApJ*, 440, 634

Rosen A., Bregman J. N., Kelson D. D., 1996, *ApJ*, 470, 839

Saha A., Sandage A., Labhardt L., Schwengeler H., Tammann G. A., Panagia N., Macchett F. D., 1995, *ApJ*, 438, 8

Satyapal S., Watson D. M., Pipher J. L., Forrest W. J., Greenhouse M. A., Smith H. A., Fischer J., Woodward C. E., 1997, *ApJ*, 483, 148

Schaerer D., Contini T., Kunth D., Meynet G., 1997 *ApJ*, 481, L75 (S97)

Schlegel E. M., 1995, *Reports on Progress in Physics*, 58, 1375

Sciortino S., Vaiana G. S., Harnden F. R., Ramella M., Morossi C., Rosner R., Schmitt J. H. H. M., 1990, *ApJ*, 361, 621

Shull J. M., Saken J. M., 1995, *ApJ*, 444, 663

Smith R. C., Chu Y. H., Mac Low M.-M., Oey M. S., Klein U., 1994, *AJ*, 108, 1266

Spaans M., Norman C. A., 1997, *ApJ*, 483, 87

Stevens I. R., Strickland D. K., 1998a, *MNRAS*, 294, 523

Stevens I. R., Strickland D. K., 1998b, *MNRAS*, in press

Strickland D. K., Stevens I. R., 1998, *MNRAS*, 297, 747

Strickland D. K., Ponman T. J., Stevens I. R., 1997, *A&A*, 320, 378

Suchkov A. A., Balsara D. S., Heckman T. M., Leitherer C., 1994, *ApJ*, 430, 511

Tenorio-Tagle G., Bodenheimer P., 1988, *ARA&A*, 26, 145

Tenorio-Tagle G., Muñon-Tuñón C., Pérez E., Melnick J., 1997, *ApJ*, 490, L179

Tomisaka K., Bregman J. N., 1993, *PASJ*, 45, 513

Tomisaka K., Ikeuchi S., 1988, *ApJ*, 330, 695

Turner J. L., Beck S. C., Hurt R. L., 1997, *ApJ*, L11

Vader J. P., 1986, *ApJ*, 305, 669

Vallenari A., Bomans D. J., 1996, *A&A*, 313, 713

Walsh J. R., Roy J.-R., 1989, *MNRAS*, 239, 297

Wang Q. D., 1995, *ApJ*, 453, 783

Wang Q., Helfand D. J., 1991, *ApJ*, 373, 497

Watson M. G., Stanger V., Griffiths R. E., 1984, *ApJ*, 286, 144

Weaver R., McCray R., Castor J., Shapiro P., Moore R., 1977, *ApJ*, 218, 377

Wilson A. S., Elvis M., Lawrence A., Bland-Hawthorn J., 1992, *ApJ*, 391, L75

Wisemann J. J., Ho P. T. P., 1996, *Nature*, 382, 139

Wrigge M., Wendker H. J., Wisotzki L., 1994, *A&A*, 286, 219

Zhekov S. A., Perinotto M., 1996, *A&A*, 309, 648